Feel free to get in contact: geo.david.fernandez@gmail.com

Anticline growth by shortening during crustal exhumation of the Moroccan Atlantic margin

Fernández-Blanco, D.[1], Gouiza, M.[2,5], Charton, R.[1,5], Kluge, C.[1], Klaver, J.[3], Brautigam, K.[4] and Bertotti, G.[1,5]

[1] TU Delft University, Faculty of Civil Engineering and Geosciences, Delft, Netherlands - corresponding author: geo.david.fernandez@gmail.com

[2] University of Leeds, School of Earth and Environment, Leeds, England, UK

[3] RWTH Aachen University, Structural Geology, Tectonics and Geomechanics, Aachen, Germany

[4] Vrije Universiteit Amsterdam, Tectonics and Structural Geology Department, Amsterdam, Netherlands

[5] North Africa Research Group (NARG)

Abstract

It is unclear how the crustal-scale erosional exhumation of continental domains of the Moroccan Atlantic margin and the excessive subsidence of its rifted domains affected the Late Jurassic-Early Cretaceous post-rift evolution of the margin. To constrain the km-scale exhumation event, we study the structural evolution of the Jbel Amsittene. This anticline is located on the coastal plain of the Atlantic rifted margin of Morocco and classically considered to have developed by Late Cretaceous halokinesis and Neogene Alpine contraction. Our structural analysis indicates that the anticline is a fault-propagation fold verging north with Triassic salts at its core and formed by shortening shortly after continental breakup of the Central Atlantic. The anticline grew by NNW-SSE to NNE-SSW shortening, as shown by syn-tectonic wedges, regional kinematic indicators and synsedimentary structures in the Upper Jurassic to Lower Cretaceous rocks. It grew further and tightened during the Cenozoic, presumably in relation to the Atlas/Alpine contraction. Our data and interpretation suggest that "tectonic-drives-salt" in the anticline early evolution, which is coeval with the growth of other anticlines along the Moroccan Atlantic margin and widespread km-scale exhumation farther onshore. Anticline growth due to shortening argue for intraplate far-field stresses, potentially linked to the geodynamic evolution of the African, American and European plates.

1 Introduction

The evolution of the Atlantic rifted margin in Morocco (Fig. 1) is marked by a period of atypically excessive subsidence during the Late Jurassic-Early Cretaceous (Gouiza 2011; Bertotti and Gouiza 2012). This early post-rift subsidence affected the distal deep basins, the continental shelf and the proximal coastal basins of the Atlantic margin, and was coeval with km-scale erosional exhumation of large continental domains to the east (Ghorbal et al. 2008; Ghorbal 2009; Saddiqi et al. 2009; Oukassou et al. 2013; Leprêtre et al. 2015a; Gouiza et al. 2017a, b). The underlying process(es) behind this exhumation are still unclear, as it took place ~30 to ~50 My after lithospheric breakup between Morocco and Nova Scotia (Klitgord and Schouten 1986; Sahabi et al. 2004) and prior to the Atlas/Alpine shortening, which gave rise to the Atlas and the Rif mountain belts (Frizon de Lamotte et al. 1991, 2008; Laville and Piqué 1992).

Similarly to other passive continental margins where comparable movements were documented in their hinterlands (Japsen and Chalmers 2000; Japsen et al. 2006, 2009; Peulvast et al. 2008; Bonow et al. 2009), these anomalous vertical movements in Morocco are likely to be driven by tectonic processes. Mechanisms proposed for the Central Atlantic include long wavelength mantle processes (e.g., dynamic topography; e.g., Hoggard et al. 2016; Müller et al. 2018), surface processes (e.g., climate driven enhanced erosion; e.g., Westaway et al. 2009), regional tectonics (e.g., rift uplifted shoulder; e.g., Ruiz et al. 2011) and horizontal far-field stresses linked to rifting onset or mid-oceanic ridge spreading (e.g., Japsen et al. 2012; Bertotti and Gouiza 2012; Green et al. 2018). Mantle processes alone, such as small-scale convection cells at the base of the mantle lithosphere, cannot explain the crustal km-scale exhumation during the early post-rift (Gouiza 2011). In this frame, attempts to link the Late Jurassic-Early Cretaceous exhumation in the east to the coeval subsidence in the west have overlooked the existence of contemporaneous NE-SW to NNE-SSW crustal shortening that might have driven both upward and downward vertical movements along the margin (Gouiza 2011; Bertotti and Gouiza 2012).

The Essaouira-Agadir Basin is located on the coastal plain of the Atlantic rifted margin of Morocco, bounded to the E and NE by the Palaeozoic basement highs of the Massif Ancien of Marrakech and the

Jebilets, respectively. These massifs have experienced substantial exhumation in the early post-rift history (Middle-Late Jurassic to Early Cretaceous; e.g., Ghorbal et al. 2008; Ghorbal 2009), while the Essaouira-Agadir Basin records clastic inputs in the Middle Jurassic and Early Cretaceous (Duval-Arnould 2019; Luber et al. 2019). The Essaouira-Agadir Basin is thus an ideal location to investigate the tectonic processes responsible for the km-scale vertical movements (Fig. 1B). Most of the compressional structures observed in the Essaouira-Agadir Basin are attributed to the Alpine shortening events leading to the uplift of the Atlas Belt (Hafid et al. 2006; Hafid 2000; Ellouz et al. 2003). Thickness changes observed in Upper Jurassic to Upper Cretaceous rocks are interpreted as resulting from synsedimentary halokinesis (Hafid et al. 2006; Hafid 2000). However, other studies show that numerous contractional structures developed during the Late Jurassic-Early Cretaceous in the western High Atlas and surroundings (Gouiza 2011; Bertotti and Gouiza 2012; Benvenuti et al. 2017).

The Jbel Amsittene Anticline is located in the central western part of the Essaouira-Agadir Basin and is one of several comparable structures within the western High Atlas basins thought to be formed by salt diapirism from the Late Cretaceous onwards (Piqué et al. 1998; Hafid 2000; Le Roy and Piqué 2001). In this work, we carry out a structural analysis of the Jbel Amsittene Anticline (Figs. 1B & 2), based on field observations in the Jurassic and Cretaceous rocks and structural modeling. We use our new evidence to discuss the tectonics of the formation of the Jbel Amsittene Anticline and its relationship with the growth of other structures in the context of the regional vertical movements recorded in the Maroccan rifted margin of the Central Atlantic.

Figure 1. Maps of tectonic provinces and geology. (A) *Regional map of Morocco showing the major tectono-stratigraphic provinces and basins of coastal Western Morocco (simplified from the geological map of Morocco; Hollard et al. 1985). With indication of the location of Panel B.* ***(B)*** *Geological map of the western High Atlas and Essaouira-Agadir Basin showing the main Triassic-Liassic rift-related structures near the Amsittene Anticline (Hollard et al. 1985; Le Roy and Piqué 2001).*

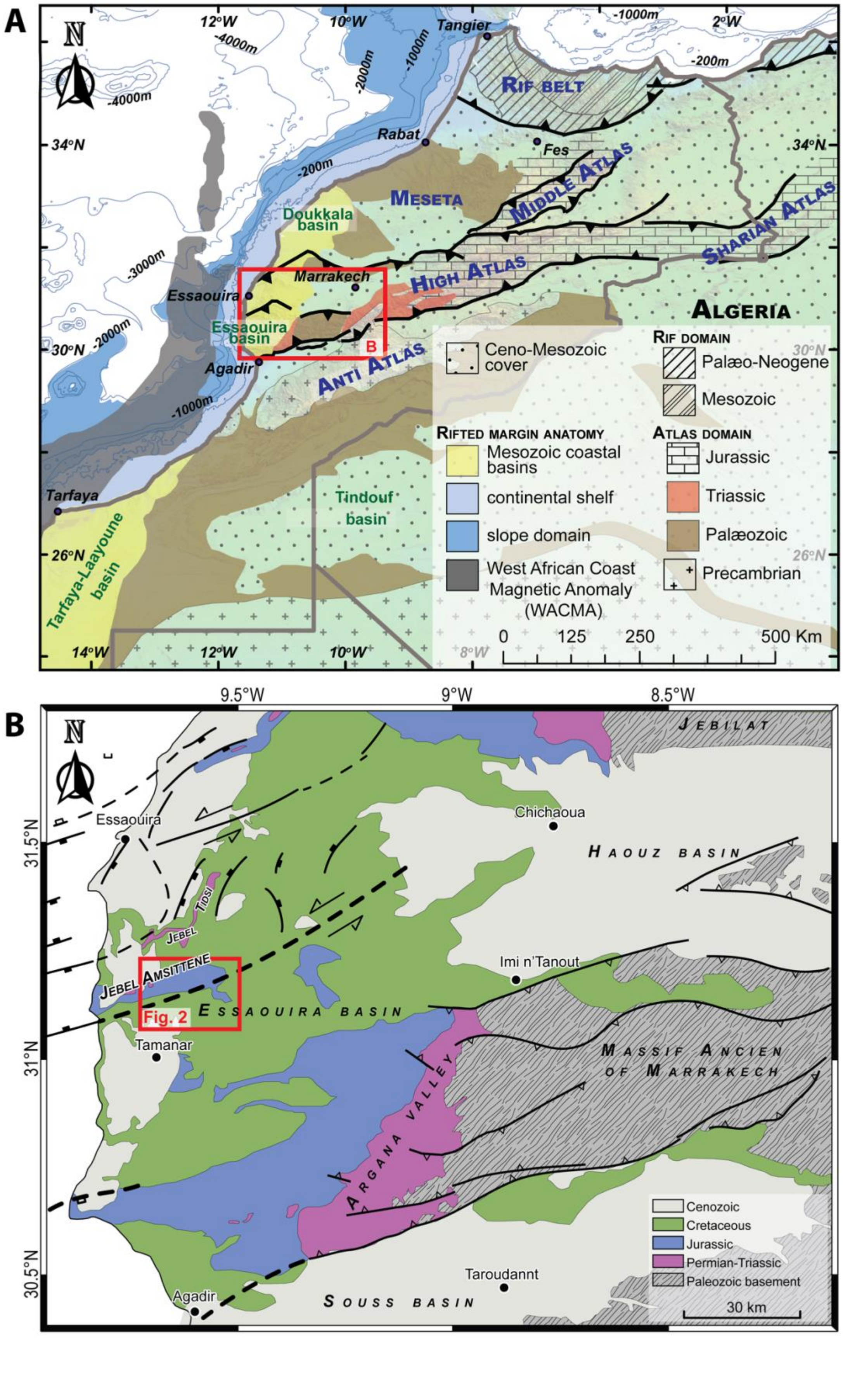
A
12°W
10°W
Tangier
-1000m
2°W
-4000m
-1000m
-2000m
-200m
-4000m
Rif belt
Rabat
Fes
34°N
34°N
-200m
Meseta
Middle Atlas
Doukkala basin
Sharian Atlas
-3000m
High Atlas
Marrakech
Essaouira
Algeria
Essaouira basin
-2000m
30°N
B
30°N
Agadir
Anti Atlas
-1000m
Ceno-Mesozoic cover
Rif domain
Palæo-Neogene
Mesozoic
Rifted margin anatomy
Atlas domain
Mesozoic coastal basins
Jurassic
continental shelf
Triassic
Tarfaya
Tindouf basin
slope domain
Palæozoic
26°N
26°N
Tarfaya-Laayoune basin
West African Coast Magnetic Anomaly (WACMA)
Precambrian
0
125
250
500 Km
14°W
12°W
10°W
8°W
B
9.5°W
9°W
8.5°W
Jebilat
Essaouira
Chichaoua
31.5°N
Haouz basin
Jebel Tidsi
Jebel Amsittene
Imi n'Tanout
Fig. 2
Essaouira basin
Tamanar
31°N
Massif Ancien of Marrakech
Argana Valley
Cenozoic
Cretaceous
Jurassic
Permian-Triassic
Paleozoic basement
30.5°N
Taroudannt
Agadir
Souss basin
30 km

2 Geological background

The Essaouira-Agadir Basin forms the western termination of the Moroccan High Atlas (Fig. 1). The basin evolved as part of the Atlantic rift during Triassic to Early Jurassic times and as a proximal shallow-water platform of the rifted Atlantic margin since the Middle Jurassic (e.g., Hafid 2000). Later convergence between Africa and Iberia/Europe since Late Cretaceous led the Essaouira-Agadir Basin in particular and the Atlas rift in general to a N-S to NNW-SSE shortening and inversion and to the build-up of the Atlas Mountains (e.g., Hafid et al. 2006; Hafid 2000; Piqué et al. 2002).

The Essaouira-Agadir Basin is composed of grabens and half-grabens bounded by N-S to NNE-SSW normal faults and E-W transform faults (Hafid et al. 2006; Hafid 2000). These extensional rift structures are filled by terrigenous red beds of Triassic age, unconformably overlain by an early Lower Jurassic evaporitic sag basin with widespread intercalations of basalt flows (Hafid et al. 2006). An early Pliensbachian unconformity, which is commonly considered to be the breakup unconformity, seals syn-rift sequences and structures (Medina 1995). Following continental breakup in the Central Atlantic, sedimentation became mostly marine in the Essaouira-Agadir Basin, leading to accumulation of a thick carbonate platform in the Middle Jurassic to Lower Cretaceous (increasing westwards from 0.5 km to 2 km; e.g., Zühlke et al. 2004), with sandstone and shale interbeds, and the deposition of Upper Cretaceous to Neogene shale-dominated series, with intercalations of limestone beds (Hafid 2000). Shortening in the Atlas domain initiated in the Late Cretaceous, leading to the formation of the Atlas fold-and-thrust belt (Frizon de Lamotte et al. 2000; Piqué et al. 2002; Teixell et al. 2003), and is believed to have triggered the formation of salt-cored anticlines in the Essaouira-Agadir Basin, with minor inversion of Triassic normal faults (Hafid et al. 2006).x

Other major tectonic events affected the Moroccan margin after the opening of the Central Atlantic Ocean in addition to the inversion and uplift of the Atlas belt (e.g. Teixell et al., 2003). Analyses of low-temperature thermochronology document a major exhumation event that affected most of the Precambrian-Palaeozoic domains exposed to the east of the Atlantic margin (i.e. Meseta plateau, Jebilet, Massif Ancien of Marrakech, Anti-Atlas belt) during Late Jurassic-Early Cretaceous times (Ghorbal et al. 2008; Ghorbal 2009; Saddiqi et al. 2009; Ruiz et al. 2011; Oukassou et al. 2013; Sehrt 2014). The Palaeozoic basement highs bounding the Essaouira-Agadir Basin, the Massif Ancien of Marrakech to the east, and the Jebilet to the northeast, experienced km-scale exhumation during the Late Jurassic-Early Cretaceous (Ghorbal 2009; Saddiqi et al. 2009). Coeval exhumation events are also documented along the margin in the Meseta plateau to the north (Ghorbal 2009; Saddiqi et al. 2009) and in the Anti-Atlas to the south (Malusà et al. 2007; Ruiz et al. 2011; Oukassou et al. 2013; Sehrt 2014; Gouiza et al. 2017b; Charton et al. 2018). This regional exhumation seems to have occurred during the post-rift stage of the Central Atlantic Ocean, i.e. ~30 to ~50 Myr after lithospheric breakup between Morocco and Nova Scotia (Klitgord and Schouten 1986; Sahabi et al. 2004), and thus, before the Atlas/Alpine contraction that gave rise to the Atlas and the Rif mountain belts (Frizon de Lamotte et al. 1991, 2008; Laville and Piqué 1992).

Jbel Amsittene is a well-exposed salt-cored anticline that strikes ENE-WSW (Fig. 2A). It is located on the coastal plain of the W Moroccan Atlantic margin, in the northwest of the Essaouira-Agadir Basin between the cities of Essaouira to the north and Agadir to the south (Fig. 1). The Jbel Amsittene Anticline has a limited extent to the west where offshore seismic data shows no folding ~10 km off the present coastline (Hafid et al. 2006).

The stratigraphy of Jbel Amssittene used in this study is based on Duffaud et al. (1966), Jaïdi et al, (1970) and Zühlke et al. (2004). The stratigraphic column shown in Fig. 2B is taken from the 1:100000 geologic map of the study area (Jaïdi et al. 1970), and shows an almost-continuous series of Upper Triassic to Lower Cretaceous rocks covered unconformably near the coast by Quaternary sediments. The oldest formation, exposed in the core of the anticline, comprises Upper Triassic (T) terrigenous sandstones and evaporites. A stratigraphic gap marks an erosional event that occurred before the deposition of open marine rocks, during the Early Jurassic (J0-J1). A gradual transition from floodplain to inner shelf environment during the Middle Jurassic (J2-J3; e.g., Duval-Arnould, 2019), resulted in a sedimentary change from predominantly siliciclastic sand-dominated units to shallow marine carbonates. The Upper Jurassic (J4-J5) sediments are mainly shallow marine carbonates of inner shelf to lagoonal environment, although there remains some sandstones and clastic interbeds (Ouajhain et al. 2011). An environmental change from inner (J/C-C1-C2) to outer shelf occurred by the end of the Early Cretaceous (C3). Quaternary terrestrial colluviums and coastal deposits overlie the Mesozoic rocks (Fig. 2).

Figure 2. Geology and chronostratigraphy in the Jbel Amsittene Anticline. *(A) Geological map of the Jbel Amsittene Anticline, showing the location of the main observations in the field and cross-sections that have been used to constrain the geological evolution of the area. Outcrops and outcrop numbers are shown as Oc.#. (B) Simplified chronostratigraphic and environmental column of the Jbel Amsittene area. Based on Hafid (2000), the geological map of Tamanar from the Moroccan Geological Survey and Zühlke et al. (2004).*

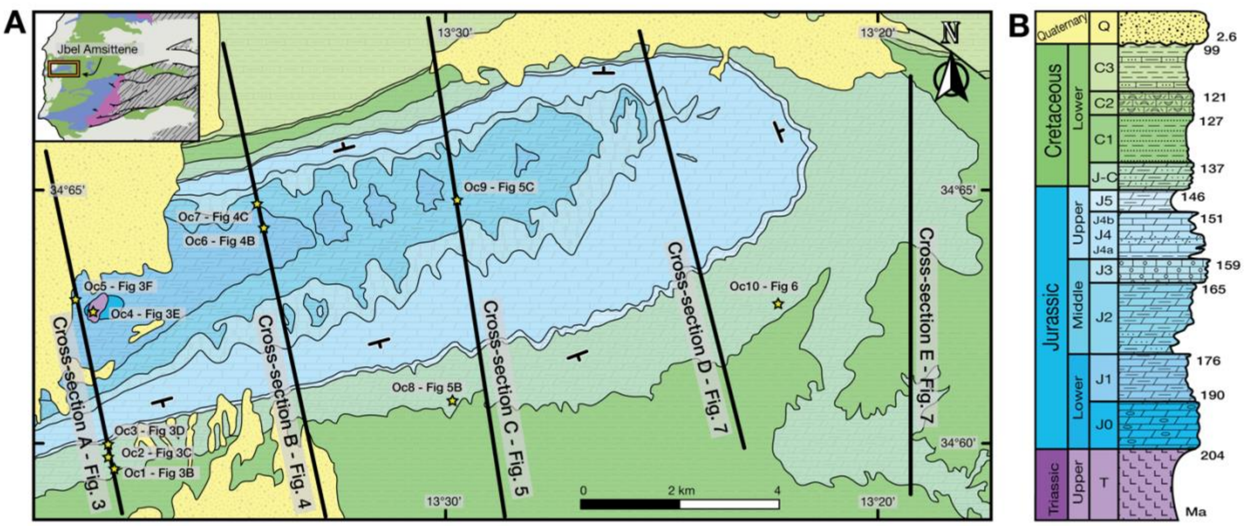

3 Jbel Amsittene Anticline geological cross-sections and field observations

We performed a detailed structural fieldwork to understand the tectonic history of the Jbel Amsittene Anticline. Whenever possible, we have differentiated strain involving soft sediments depositing during the early post-rift of the Central Atlantic that provide key information on the stress field during growth of the structures (especially in the Late Jurassic - Early Cretaceous), from observations of strain related to Alpine events that are presumably Cenozoic. We show relevant and representative outcrops (Fig. 2A) that summarize the main structural observations along three cross-sections. We provide uninterpreted pictures of these outcrops and complementary pictures in the Supplementary Material.

The geological cross sections are located roughly 4 km apart transecting the anticline across its axis, NNW-SSE, and were constrained by bed measurements and field observations. Cross-section A (Fig. 3) is parallel to a road-cut for most of its length, which results in the best rock exposures in the area. Jurassic and Cretaceous rocks outcrop in the south and central parts of the profile and are covered by Quaternary deposits in the northern region. Cross-section B (Fig. 4) is located ~4 km east of cross-section A and runs parallel to it. Cross-section B is often covered by vegetation and has poor accessibility with a small number of well-preserved outcrops. Cross-section C (Fig. 5) runs parallel to previous sections, and is located ~4 km east of cross-section B. We also reproduced two additional sections and describe an outcrop located farther east. Finally, we describe and recapitulate information relevant for the discussion in the form of along-strike and across-strike lateral variations, syn-sedimentary deformation, and a 3D thickness model.

3.1 Western profile: Cross-section A

The lower Lower Cretaceous (C1) to lower Middle Jurassic (J2) layers dip south in most of the southern flank and change from horizontal to steeply north-dipping where the topography is the highest. North of the topographic high, layers dip south again and finally outcrop as overturned, prior to being covered by Quaternary deposits in the northernmost area of the section. Quaternary rocks prevent an unambiguous thickness comparison between the older units on both sides of the anticline. Those that could be compared showed no changes in thicknesses. The transition from horizontal to overturned layers is observed in the oldest Jurassic rocks exposed in this section (lowermost Jurassic, J1). The dip of the stratigraphic layers indicates a northward verging anticline with a tête-plongeante (plunging head) shape (sensu Seguret 1972) in its central-northern sectors.

Lower Cretaceous rocks dip gently to the south (10˚-20˚) in the southernmost part of the southern flank (“a” in Fig. 3A), and become steeper towards the north, reaching dips of ~80˚ at the highest point of the topography. Changes in dip are not constant and north dipping layers outcrop in the central sector of the southern flank (Fig. 3A), within the middle and lower Upper Jurassic rocks (J4). Moving northwards, the dip of the layers locally changes in relation to secondary N-verging folds tens of meters in size. Three conjugate fault sets outcrop in a local topographic flat in the uppermost Upper Jurassic-lowermost Lower Cretaceous (J-C) limestones (Oc1; Fig. 3A, 3B; Table 1). The regional bedding dips gently to the SSE, and the three conjugate fault sets show clear striations of sub-horizontal to gently S directions (216/04 and 171/20). The fault planes and associated striations are indicative of N-S to NNE-SSW maximum horizontal stresses, both for rocks rotated with respect to the regional bedding (post-tilted) and non rotated (pre-tilted). From this outcrop northwards, bed dips start to increase and reach values up to ~55˚ toward the south ("b"; Fig. 3A). Less than 50 m before the exposure of the lower Lower Cretaceous rocks (C1), a N-S-striking sub-vertical clastic dyke of marine clastics cuts S-dipping strata (Oc2; Fig. 3C). A few meters northwards, a syn-sedimentary N-verging ramp fold indicates soft sediment deformation (Oc3; Fig. 3D). Whereas the conjugate fault sets in Oc.1 (Fig. 3B) suggest no deformation took plane before deposition of uppermost Upper Jurassic – lowermost Lower Cretaceous unit (J-C), the latter two synsedimentary structures (Oc2; Oc3, Figs. 3C, 3D) indicate NNW-SSE shortening during its deposition.

Figure 3. Western profile and main outcrops. *(A) Cross-section A. (B) Outcrop 1. Limestones with regional bedding shown in yellow and faults and fault planes shown in red, with striae in dashed stroke. Conjugate sets and their stress directions indicate a north to south to north-northeast to south-southwest shortening. The steepness of the faults may indicate reactivation. (C) Outcrop 2. Neptunian clastic dyke of calcarenite shown in red intruded in limestone with regional bedding shown in yellow. The neptunian dyke has a present position of 272/83. Assuming horizontal bedding at the moment of deposition, the neptunian dyke developed vertically, and is an indicator of east-west extension. (D) Outcrop 3. Folded and faulted soft sediments in a syn-sedimentary ramp fold, verging north, indicating shortening in a 160-340 direction during the 144-150 Ma (latest Jurassic). Limestone showing regional bedding to the left and folded strata to the right (in yellow) and a reverse fault (in red). The soft sedimentary packet (with a sedimentary pattern) shows a chaotic character with no evidence of brechiation. (E) Outcrop 4. Map of the salt outcrop in the west and adjacent formations, showing the bedding strikes around the evaporitic body. (F) Outcrop 5. Reverse faults and folds with southeastern vergence, in a limestone outcrop situated less than 200 meters east of the outcropping salt. Regional bedding to the right and folded strata to the left are shown in yellow and reverse faults are shown in red. Rocks in the outcrop are not affected by halokinesis, and show signs of compressional deformation. The orientation of the fault planes and the axial planes of the folds are similar and indicate NNW-SSE shortening.*

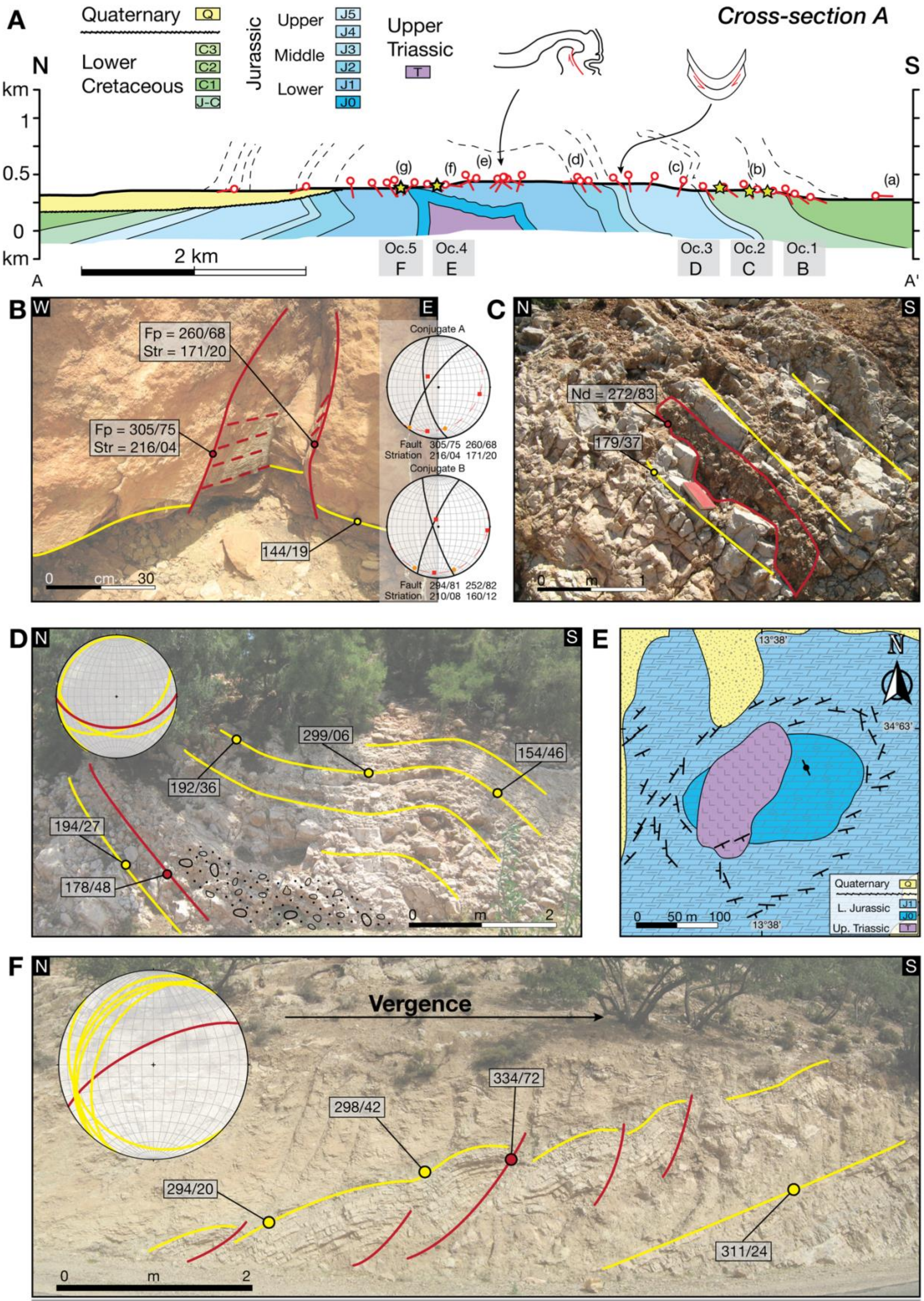

A
Cross-section A
Quaternary Q
Lower Cretaceous C3 C2 C1 J-C
Jurassic Upper J5 J4 Middle J3 J2 Lower J1 J0
Upper Triassic T
N
S
km
1
0.5
0
km
(a) (b) (c) (d) (e) (f) (g)
2 km
Oc.5 F
Oc.4 E
Oc.3 D
Oc.2 C
Oc.1 B
A
A'
B
W
E
Fp = 260/68
Str = 171/20
Fp = 305/75
Str = 216/04
144/19
0 cm 30
Conjugate A
Fault 305/75 260/68
Striation 216/04 171/20
Conjugate B
Fault 294/81 252/82
Striation 210/08 160/12
C
N
S
Nd = 272/83
179/37
0 m 1
D
N
S
299/06
154/46
192/36
194/27
178/48
0 m 2
E
13°38'
34°63'
N
0 50 m 100
13°38'
Quaternary Q
L. Jurassic J1 J0
Up. Triassic T
F
N
S
Vergence
334/72
298/42
294/20
311/24
0 m 2

205

Table 1. *Orientation of the main stresses derived from Outcrop 1 (Fig. 3B).*

Bedding	Present orientation			Orientation before tilting		
	σ_1	σ_2	σ_3	σ_1	σ_2	σ_3
144/19	010/09	256/68	103/20	014/22	208/67	106/02
144/19	183/01	282/81	093/09	005/13	171/76	274/03
146/28	203/28	344/56	103/18	195/11	031/79	286/03

Structures north of these outcrops seem to be exclusively related with the Alpine deformation phase. Approximately 200 m north of these outcrops, the Upper Jurassic layers (J5) dip north ("c" in Fig. 3A). Steep and sub-vertical N-dipping overturned layers alternate on occasion with S dipping beds with similar attitudes ("d") for ~400 m in lower and middle Upper Jurassic rocks (J4). Bedding-parallel flexural slip associated with Alpine deformation is common and related striations show a N-S slip direction. Northward, Middle Jurassic (J3-J2) strata dip consistently south until the topographic profile reaches its highest elevations ("e"). North of the topographic high, the orientation of Lower Jurassic strata (J1) changes from subvertical (~80˚) to subhorizontal with a gentle S-dip within a distance of ca. 500 m (Fig. 3A). Between the sub-vertical and sub-horizontal Lower Jurassic (J1) layers, S and N dipping sub-vertical strata alternate. Within this sector ("f" in Fig. 3A), highly deformed structures appear, showing faulted and folded strata, m-folds, recumbent folds, fault-related-folds, and more complex features, with unclear or non-sequential vergence. More to the north, the strike of the Lower Jurassic strata show no consistent trend for ~300 m, and outcrop as overturned (up to ~60˚) or S-dipping layers. Around 300 m east off the section, Upper Triassic evaporites (T) outcrop in a circular depression of approximately 1 km in diameter (Oc.4; Fig. 3E). An intrusive contact is seen between the evaporites and the lowermost Jurassic unit (J1). The Lower Jurassic bedding dips away from the outcropping evaporites, from sub-vertical nearby to 25˚ farther away from them. The strike directions of these Jurassic rocks vary consistently around the salt, in an overall concentric configuration. The strike directions progressively change to the regional E−W to SW−NE trends 300-400 m away from the evaporites. Continuing north along cross-section A, overturned strata become subvertical (80˚-85˚) ("g") and finally N-dipping, before reaching the sub-horizontal Quaternary (Q) rocks that discordantly cover most of the northern flank. In this area, a sequence of SSE-verging fault-propagation folds outcrops in the Lower Jurassic (J1), with axial planes indicating a SSE-to-NNW shortening direction (Oc5; Fig. 3F).

3.2 Central profile: Cross-section B

Gently south dipping lower Lower Cretaceous (C1) to lower Middle Jurassic (J2) layers outcrop from the southern side of the anticline until significantly north of the topographic high (Fig. 4A). The oldest rocks seen in the section are Lower Jurassic (J1) and outcrop ~1,5 km north of the topographic high, in the core of the anticline. North of the hinge of the anticline there are steep north dipping layers of lower Middle Jurassic (J2) to Lower Cretaceous (C1) age. Some of these steep layers are overturned and dip south ("i" in Fig. 4A). Further north, the Lower Cretaceous strata (C2-C3) have gentle north dipping slopes. The uppermost Upper Jurassic to lower Lower Cretaceous (J-C to C1) rocks are significantly thinner in the northern (~350 m) than in the southern (>900 m) flank along cross-section B (Fig. 4A).

In the southernmost of cross-section B, Quaternary (Q) deposits cover Lower Cretaceous rocks (C1-C3) ("a" in Fig. 4A). Northwards, rocks of the uppermost Upper Jurassic to lower Lower Cretaceous (J-C to C1) outcrop with consistent dips of ~40° to the south ("b"). Upper Jurassic (J4-J5) layers have steeper dips that vary from ~40° to ~65° to the south ("c"). Further north, the Middle Jurassic (J2-J3) layers gradually decrease in steepness from ~45° to ~35° to the south ("d") and become roughly parallel to the topography ("e", dips of 10°-20° to the south) as they reach the topographic high.

Starting 300 m northwards of the topographic high, ~20° to 40° south dipping layers alternate with ~40° north dipping layers. This trend continues for ~400 m, and is seen also for part of the Lower Jurassic (J1) rocks ("f"). Layers are folded asymmetrically in this area until the northward dips become dominant (Oc.6; Fig. 4B). Advancing farther north, these Lower Jurassic (J1) layers overturn and dip south again, for a distance of more than 900 m. Lower Middle Jurassic (J2) overturned layers outcrop showing the largest overturn along this profile (175°/73°) ("g"). These Jurassic rocks are locally underthrusted in a fault-bend fold structure that indicates top to the south motion (Oc.7; Fig. 4C). The layers remain sub-vertical for around 1100 m, and gradually decrease in steepness, from ~85° to ~50° to the north, in the lowermost Cretaceous (J-C) unit (“h”). Toward the north, layers of the lowest Lower Cretaceous (C1) are sub-vertical again, while the middle Lower Cretaceous (C2) strata have shallower dips (40° N) (“i”) that decrease gradually to 20° N when reaching the upper Lower Cretaceous (C3) rocks. Observations show no evidence of synsedimentary deformation in the rocks of uppermost Upper Jurassic to lower Lower Cretaceous (J-C to C1) age along the cross-section B, but these units show a decrease of >500 m in thickness across the anticline strike (Fig. 4A).

Figure 4. Central profile and main outcrops. *(A) Cross-section B. (B) Outcrop 6. Meter-scale fold in limestones at the location of main dip change in beds (shown in yellow) at the anticline axis. (C) Outcrop 7. Underthrust in overturned limestone strata. The fault is in red and beds are in yellow. Fault-bend fold, with top to the south movement, with 175/73 regional bedding. The fold in the hanging wall has a fold axis of 085/06 and axial plane of 022/14.*

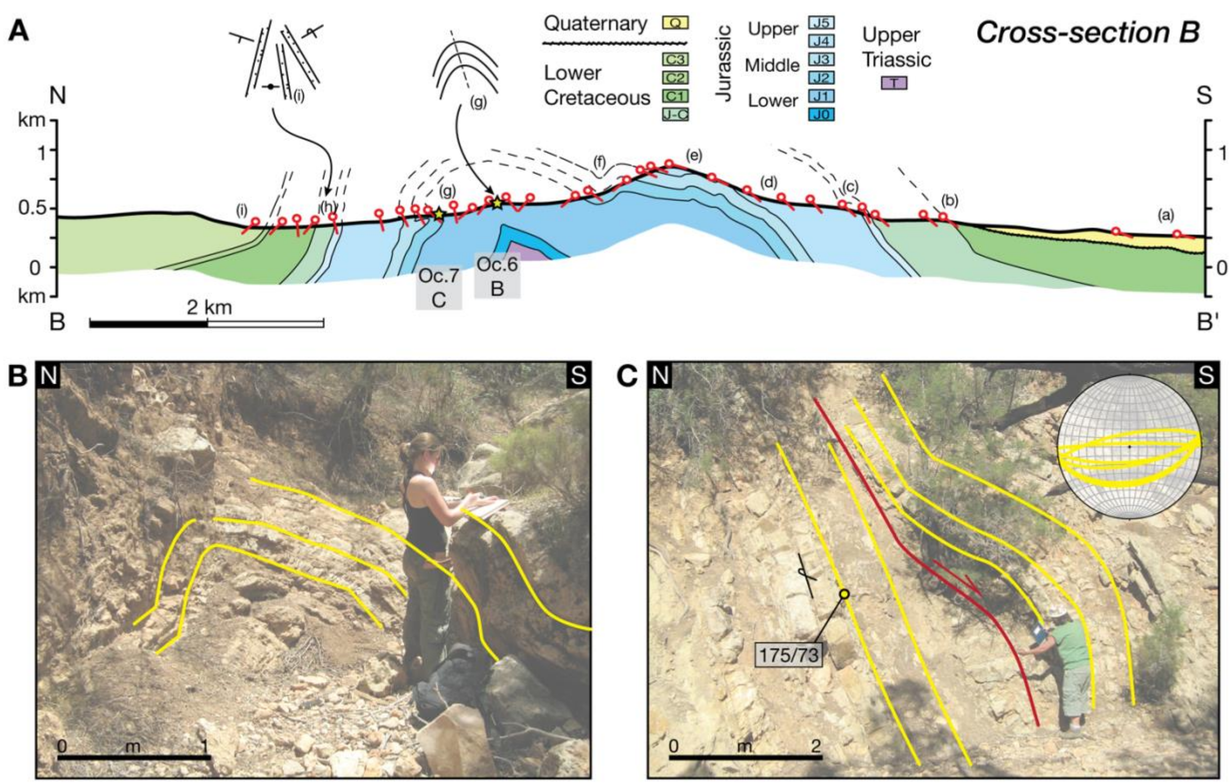

3.3 Eastern profile: Cross-section C

Cross-section C portrays a north vergent anticline with two hinges, showing a northern steeply dipping flank and a southern gently dipping flank (Fig. 5A). The rocks exposed along this easternmost section are early Middle Jurassic (J2) to late Early Cretaceous (C3) of age. The thickness of the lowermost Cretaceous (J-C) formation varies from approximately 550 m on the southern flank to 400 m on the northern flank of the anticline, whereas the thicknesses of the Jurassic formations J2 to J5 are constant along the profile.

In cross-section C, the southern flank of the Jbel Amsittene Anticline is characterized by south dipping sedimentary beds ("a" in Fig. 5A), with subhorizontal Cretaceous rocks in its southernmost sector. Towards the north, older south-dipping rocks crop out. Within the lowermost Lower Cretaceous – uppermost Lower Jurassic formation (J-C), layer inclinations vary between approximately 30° and 80° to the south ("b"). Here, the layers are locally offset by cm to dm-scale reverse faults, which indicate N-S to NNE-SSW shortening coveal with sedimentation. Outcrop 8 (Fig. 5B) shows an example of these reverse faults in limestones. SSW dipping faults in this outcrop have up to ~20 cm offset and terminate in the slumped overlying sediments that show soft deformation, indicating a possible phase of syn-sedimentary deformation during the early post-rift of the Central Atlantic.

Outcrops farther north evidence deformation due to Alpine shortening. Towards the topographic high, the dip of the bedding gradually decreases from ~40° to 20° to the south, and upper Middle to middle Upper Jurassic (J3 – J4) rocks are exposed ("c"). Calcite-filled tension gashes are observed in several outcrops in and around the topographic high (Oc. 9; Fig. 5C). The veins are spaced by few cm, and show both top-to-the-north and top-to-the-south shear kinematics. The former occurs mostly to the south of the topographic high, and the latter is observed mainly to the north of the topographic high. Northwards, along a ~500 m sector, the beds are subhorizontal gently dipping to the north ("d"). Approximately 1 km farther north, beds dip to the south for ~100 m before dipping north again ("e") and lower Middle Jurassic (J2) rocks are exposed. In the second topographic high, where the second hinge plane of the anticline intersects the topography, the orientation of the bedding is 65° to the north ("f"). Between the second topographic high and the valley north of the Jbel Amsittene Anticline, successive upper Middle Jurassic (J3) to lower Lower Cretaceous (C1) strata are exposed steeply dipping north (60-80°) ("g"). North of the valley, Lower Cretaceous (C1 to C3) strata are exposed dipping ~10 to 20° northwards ("h").

Figure 5. Eastern profile and main outcrops. *(A) Cross-section C. (B) Outcrop 8. Inclined limestone layers cut by synsedimentary faults. High-angle reverse faults (in red) transect a thick bank (with its top and its bottom beds in yellow) with an offset of ~20 cm. The reverse fault tips end in the sedimentary layer on top that show soft sediment deformation of chaotic nature (in thin black), bracketing the age of deformation to 146-137 Ma (J-C formation, lowermost Lower Cretaceous – uppermost Lower Jurassic). The inclination of the reverse faults is suggestive of reactivation of former normal faults. (C) Outcrop 9. One of the two sets of sigmoidal tension gashes that outcrop at both sides of one of the anticline axes, in limestones. They indicate right lateral shear.*

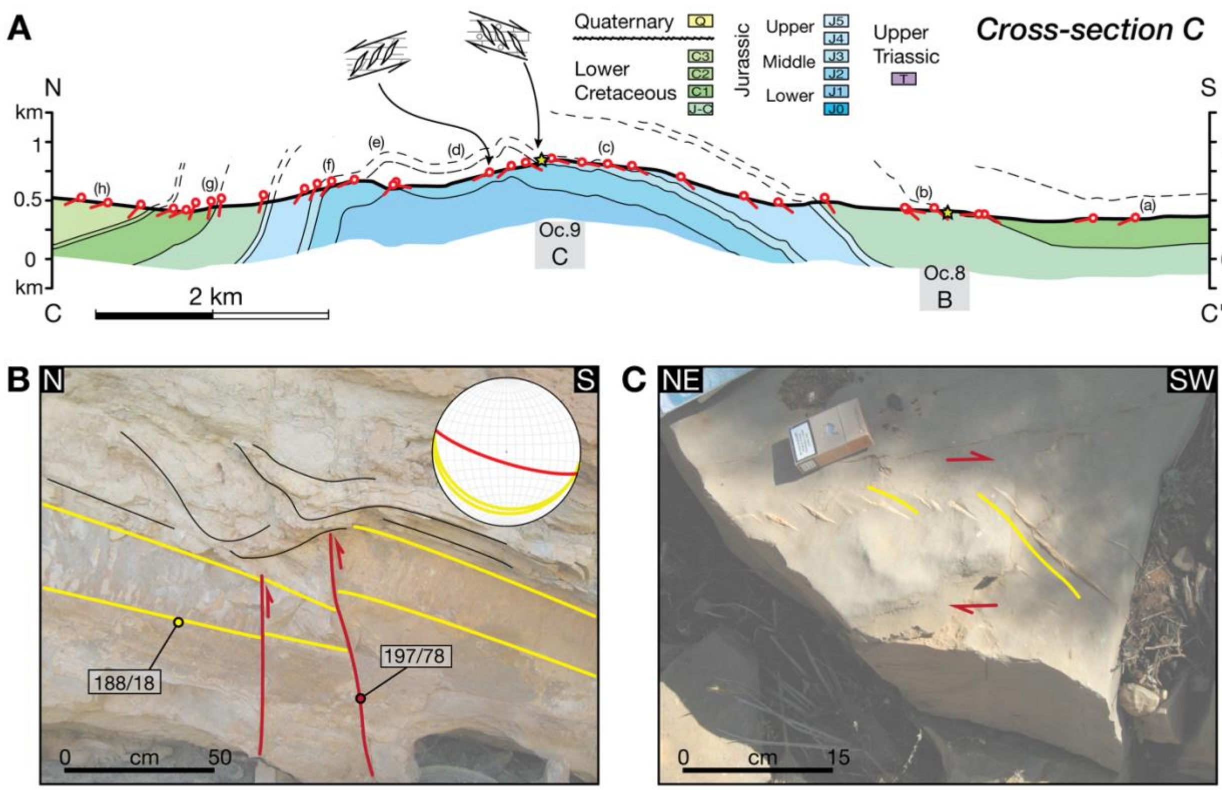

3.4 Eastern sectors of the Jbel Amsittene Anticline

Other relevant structural observations were found eastwards of the above-described sections. The most relevant structure for the scope of this study outcrops ~5 km to the east of cross-section C, in the lowermost Cretaceous (J-C) limestones (Oc. 10; Fig 6). This outcrop depicts a series of high angle reverse faults dipping SSW that transect limestones below a ~30 m long sedimentary wedge that pinches out towards the

S. The top-to-the-north faults show reverse offsets of few to tens of centimeters and slickenlines indicating SSW-NNE shortening direction. The upper terminations of the faults are within the overlying lowermost Cretaceous syn-tectonic strata, and indicate active deformation during this period.

Figure 6. Outcrop 10. *Limestone outcrop showing an approximately 30 m long wedge pinching out towards the south, overlaying faulted strata. The top to the north-northeast faults have reverse offsets of a few to tens of centimetres that do not continue into the wedge, indicating a shortening direction of SSW-NNE during the J-C formation, lowermost Lower Cretaceous – uppermost Lower Jurassic. The steepness of the faults may be indicative of reactivation.*

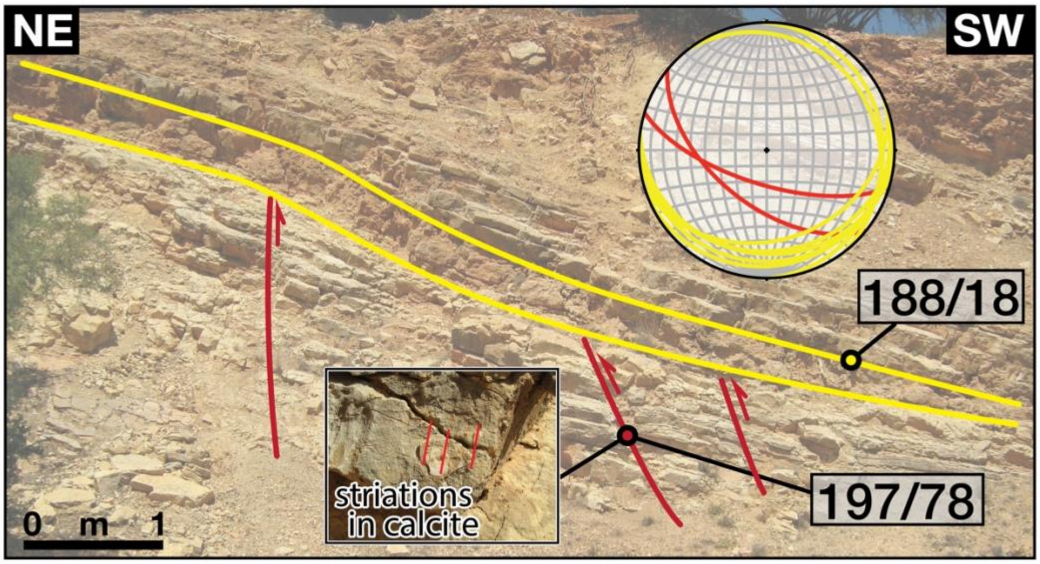

3.5 Structure and lateral variations in the Jbel Amsittene Anticline

We produced a structural map of the Jbel Amsittene (Fig. 7A), reconstructed two sections further east, where the anticline is more open (shown in Fig. 7B), and other sections to the west (not shown). These sections are similar in overall structure and geometry and change relevantly, albeit continuously, along the strike of the anticline (Fig. 7). The eastern profiles (bottom of Fig. 7B) depict an open and asymmetrical anticline with a gentle north vergence. In the eastern profiles (i) the southern limb dips gently and persistently south, (ii) salt deformation is not noticeable, neither in the hinge nor elsewhere, and (iii) the northern limb shows north dips with no overturned strata. The anticline shows a well-confined hinge and its flanks dip more gently than their western continuations. Small-scale structures are rare and more open

324 ***Figure 7. Structure of the Jbel Amsittene Anticline.*** *(A) Structural map showing the main axis of the anticline, which bifurcate*
325 *westwards, and its plunge towards the east. The also shows regional bed attitude representative of different sectors of the anticline.*
326 *We provide all bed dip data from the fieldwork in the Supplementary Materials. Contours in grey represent lines of equal height*
327 *every 50 m, with darker tones and thicker strokes for the heights of 250 m, 500 m and 750 m. (B) Geological profiles in the Jbel*
328 *Amsittene Anticline, from west to east, showing the anticline structure and vergence and its lateral variations.*

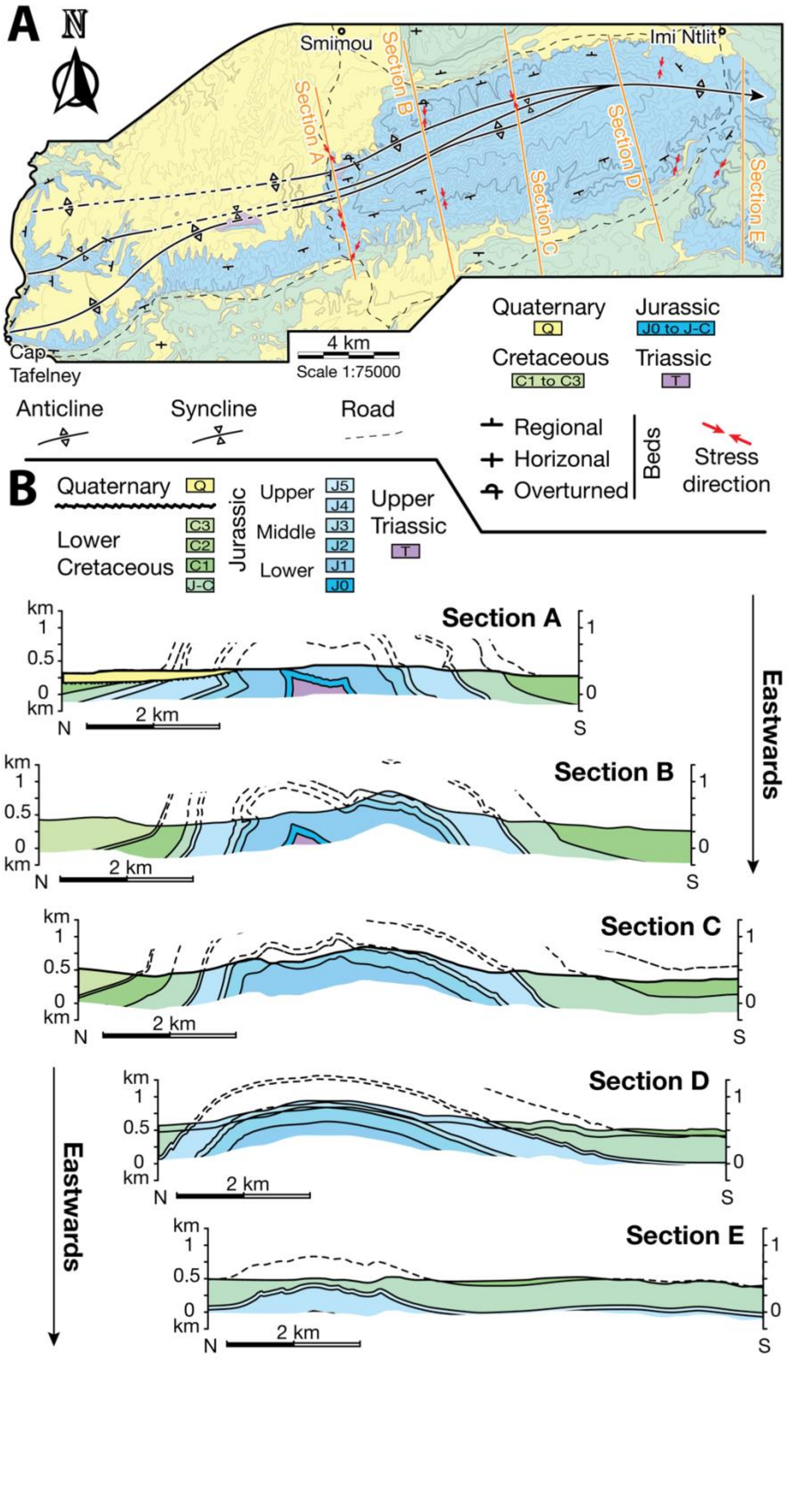

329

in character. The layers along the limbs alternate sectors of constant dip with others where they vary progressively. By contrast, the western profiles (top of Fig. 7B) present a tight structure and a clear north vergence. In the western profiles, (i) the southern limb of the anticline dips south, from gently to steep, with local dips to the north, (ii) distortion by diapirism is limited to near the hinge where the salt is outcropping, and (iii) the northern limb is frequently overturned and partly covered by Quaternary deposits. The western profiles show a topographic crest characterized by a north tête-plongeante geometry. Strain markers are numerous and strata often show relevant changes in dip direction over short horizontal distances.

3.6 Thickness changes along the Jbel Amsittene

To obtain thickness variations in the Jurassic formation, we put forward a 3D thickness model integrating remote sensing (horizon mapping) and structural data (dip data and geological cross sections; Fig. 8). We have used a "3 point-solver" plug-in for Google EarthTM to derive bed attitude from their contact with topography at three or more points (Bennison and Moseley 2003) and collect large-scale dip data at various locations around the anticline. We mapped horizons on DEM-coupled satellite images (Google Earth ProTM) to obtain spatial coordinates of well-exposed geological contacts, identified by the georeferenced geological map of Choubert (1965) and color changes in the imagery. We used the mapped horizons and the large-scale (tens of meters) dip data in geological cross-sections to derive a 3D model of continuous stratigraphic surfaces using *Gocad StructuralLab* tool. We then obtained true thickness maps by means of the *kine3d-1* tool that we extracted in the vicinity of mapped horizons using *Matlab*. Model resolution suggests a precision of ~20 m at the surface, and hence lies below the thinnest stratigraphic units within the study area.

Thickness maps reveal an along-strike change in the thickness of Jurassic rocks (Fig. 8). Thickness variations comprise the Lower Jurassic (J0, J1), Middle Jurassic (J2, J3), and Upper Jurassic (J4, J5) along a clockwise profile from the northwestern to the southwestern fold flanks. We find maximum unit thicknesses in the overturned northern flank and a decrease in thicknesses eastwards. Such thickness decrease is substantial at the point where the fold limbs change into NNW dipping beds. All formations follow this trend, that becomes less significant towards the Upper Jurassic (J4, J5). It is worth noticing, however, that modeling is less precise in overturned layers. In the southern limbs, towards the west, thicknesses in all formations increase progressively, albeit remaining below thicknesses of the northern limb (Fig. 8). Generally, thicknesses are never constant along the anticline strike for >5 km. Thickness at the eastern side are around 40 to 50 m in J3 and 140 m and 80 m in J4, respectively. Sediments increase in thickness towards the southern limbs, with 140 m to 200 m for J3. This corresponds to a thickness increase of ~70-75%. The J4a (Oxfordian) strongly increases from around 140 m to more than 300 m.

Figure 8. Thickness model. *(A/B/C) Model of thickness variations along contour likes of three Upper Jurassic sequences. (D) Modelled thickness variations of Jurassic rocks in a clockwise profile from the northwestern to the southwestern flank of the anticline.*

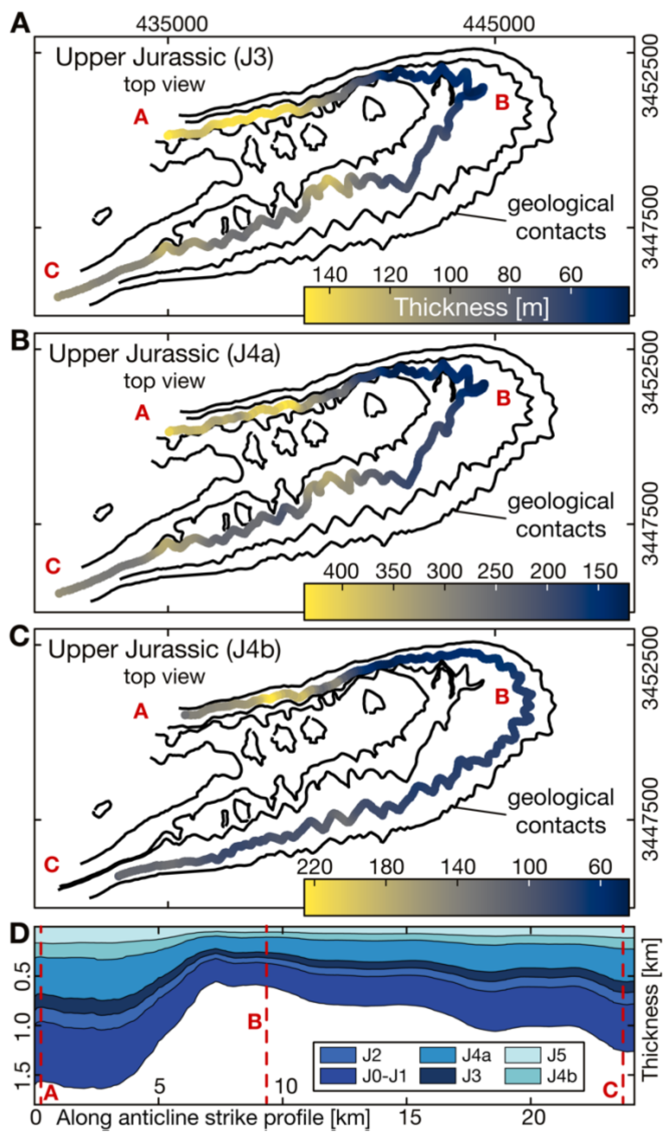

We also derive thickness for the upper Upper Jurassic - Lower Cretaceous units (J-C, C1, and C2). For this case, we derive thicknesses from the attitude of beds within the units and along their contacts. We use this input to infer the planes of contact between the sedimentary units and calculate true thicknesses by measuring the distance between contacts orthogonally. Although this approach is less accurate and lacks the along-strike coverage of the aforementioned thickness model, it provides a valid first-order signal on the across-strike variation of sedimentary thickness. The upper Upper Jurassic - Lower Cretaceous units (J-C, C1, and C2) decrease in thickness northwards across the strike of the Jbel Amsittene Anticline (Table 2). As seen in cross-sections A and B (Figs. 4 & 5), formations J-C and C1 are up to ~350 m thinner in the northern flank with respect to the southern flank of the anticline (Table 2). These values represent a minimum estimate, given that the upper boundary of C1 is in places outside the limits of our study area. Our observations suggests that sedimentary thickness changes also affect also C2, and that no thickness changes affect the Lower Cretaceous C3 formation. These thickness variations are less obvious in the east of the study area (Fig. 7).

Table 2. *Thickness changes between the northern and the southern flank of the Jbel Amsittene Anticline for formations J-C and C1.*

	Formation J-C		Formation C1	
	N flank	S flank	N flank	S flank
Cross-section B	150m	500m	350m	500m
Cross-section C	400m	650m	350m	450m

4 Discussion

4.1 Key characteristics of the Jbel Amsittene Anticline

The Jbel Amsittene Anticline has a limited lateral extent and shows geometry changes along strike (Fig. 7). In the west, the anticline manifests as a box anticline with a gentle north vergence within a broader area of deformation. The anticline continues westwards into the offshore for less than ~10 km off the coastline

(Hafid, 2006). The tight tête-plongeante that the anticline has in the west smoothens and widens into an open fold (up to ~20 km in wavelength) and wanes eastward, as the axis of the anticline plunges eastwards (Fig. 7). As a result of an eastward plunge of the fold axis and the southward dip of its axial plane, the oldest rocks at the core of the anticline are exposed in the west and located to the north of the topographic high.

Thickness variations have different trends in Jurassic and Early Cretaceous units. Jurassic units show a signal of eastward decreasing thicknesses along strike and with maxima in the anticline center (Fig. 8). The cumulative thickness for the Jurassic units has sharp variations of up to 900 m between the northern flank and the eastern termination of the anticline, while between the latter and the southern flank, thickness variations are of ~600 m. A second-order signal across the anticline strike portrays a decrease in thickness towards the southern flank (Fig. 8). Sedimentary units J-C and C1 have thicknesses that decrease up to 500 m northwards across the strike of the anticline, in turn decreasing eastwards some 150 m over short horizontal distances (Table 2). Whereas thickness changes in Jurassic units seem unrelated to a tectonic event, the latter units may relate to changes in shortening rates (see below).

Differential strain distribution along the anticline strike can be inferred for modern and antecedent forms of the Jbel Amsittene Anticline. We derive these along-strike changes in the amount of shortening from the variations in line-length approximations along the present anticline strike and from the number and size of outcrop-scale syn-sedimentary structures in the Upper Jurassic – lower Lower Cretaceous (J-C) formation (Table 3). The western profile presents shortening values of ~1,6 km over a measured length of ~7,6 km, i.e., ~21% shortening. This shortening value remains almost constant in the central profile (~20 %), and decreases in the eastern profile (14,5 %). Farther east, in the easternmost section, we measured 0,2 km of shortening over a length of ~4,3 km, i.e. ~4,5 % shortening (Table 3). Thus, line-length shortening decays along the Jbel Amsittene Anticline strike from its center to the east. Although most deformation and probably the observed eastward decay in shortening along the anticline strike relates to structure tightening during Alpine times, we infer a similar trend for the syn-depositional structures in the Upper Jurassic –

lower Lower Cretaceous (J-C) formation. Most of such syn-depositional structures appear in the west of the anticline and are absent in coveal rocks in the east and of upper Lower Cretaceous (C3) age exposed in the northern part of the study area. This suggests that decreasing-eastwards shortening resulted in the growth of an anticline with an open geometry by the end of the Lower Cretaceous (C3).

Table 3. *Decrease in amount of shortening to the east, measured as unfolded line-length.*

	Deformed length (km)	Shortening (km)
Cross-section A	7,6	1,6
Cross-section B	9,5	2,1
Cross-section C	10,3	1,5
Cross-section D	9,1	0,6
Cross-section E	4,3	0,2

Syn-sedimentary deformation is common in outcrops of the uppermost Upper Jurassic-lowermost Cretaceous limestones (J-C), and is expressed as clastic dykes, fault-related folds and reverse faults affecting soft sediment (Figs. 3, 4, 5 & 7). Overall top-to-the-north steep reverse faults with tips that offset soft sediments by few to tens of centimeters (Figs. 5 & 6) suggest N-S to NNE-SSW shortening. This observation can be coupled with striae in nearby conjugate fault sets indicating NNW-SSE to NNE-SSW maximum horizontal stresses (Fig. 7). Other equivalent coeval reverse faults are also steep in their pre-rotated stages, and probably result from reactivation of Triassic–Liassic normal faults. Similar evidence of syn-sedimentary shortening during deposition of the J-C unit can be found along the anticline strike. However, regional layer dips for this unit vary greatly (between approximately 30° and 80°), and evidence in other outcrops, such as the tête-plongeante or the overturned strata, are clear indications of younger shortening. Taken together, the data suggest that shortening during the early post-rift phase of the Central Atlantic initiated anticline growth of the Jbel Amsittene, and that the anticline further developed and tightened during the Alpine orogeny (e.g., Saura et al. 2013 in the Central High Atlas; Pichel et al. 2019b in the offshore Essaouira-Agadir Basin; this study, in the Jbel Amsittene).

4.2 Models for the evolution the Jbel Amsittene Anticline

We put forward two potential models for the evolution of the Jbel Amsittene Anticline in Mesozoic times. We discuss, on the basis of the evidence presented in this contribution, our preferred model for such initial anticline development, which was enhanced and partly overprinted in the Cenozoic. Comparative, detailed structural studies inclusive of similar onshore anticlines in the area are required to confidently discriminate among these two potential evolutionary models proposed for the Jbel Amsittene Anticline, and elucidate the underlying growth mechanism for equivalent structures in the Moroccan margin. Discrimination among different models in turn would have implications on the geodynamic causes controlling the anomalous vertical motions during the early post-rift phase along the African margin.

In a first scenario, we assume that the Triassic salt at the core of the present anticline is the driving force leading anticline growth already during the Early to Middle Jurassic. Halokinesis and salt tectonics are well expressed in the area (Hafid et al. 2006; Hafid 2000) and proposed to happen during this period in the Central High-Atlas (Saura et al. 2013) and in the offshore Essaouira-Agadir Basin (Pichel et al. 2019a). Although extensive diapirism exist offshore Morocco, no clear interpretations of pre-Cretaceous timing and mechanism(s) of salt mobilisation are available, and it thus may occur in relation to different mechanisms than in the onshore (Neumaier et al. 2016). Moreover, salt mobilisation may potentially lead to syn-sedimentary deformations along the sides of the diapir and sedimentary dykes (Morley et al. 1998; Giles and Lawton 2002 respectively; see examples in Poprawski et al. 2014). The Late Jurassic-Early Cretaceous deformation features may therefore be gravity-driven sedimentation features of local origin that can form on any submarine slope of a few degrees.

All syn-sedimentary faults observed in the field are very steep. Although this might be the result of fault measurements concentrating on the steep, upper tips of the faults, none of the faults has its root exposed. Moreover, the upper tips seem to show a sharp termination, potentially lithology-controlled. Is it possible that all of these faults are intraformational, and that they, and folded units, were generated by shear stresses of individual sedimentary packages sliding along bedding planes. This could be associated with slope gravity processes, or a rising salt diapir. Slope oversteepening can be purely sedimentary, and tectonic processes do not have to be involved to explain their formation. In this scenario, vertical movements (Stets 1992; Bertotti and Gouiza 2012; Gouiza et al. 2017b) could be linked to anticline fold growth and salt tectonics, such that a gravitational load is applied by the uplift of the High Atlas and by the subsiding continental margin, creating a hydraulic head and consequent salt activation (Pichel et al. 2019a). The presence of salt in the anticline core and Jurassic thickness variations along the anticline that do not relate to the present structure are potential indicators for such salt-driven scenario, although further evidence from nearby anticlines need to be found.

In a second scenario, we assume that the Jbel Amsittene Anticline initially formed by horizontal shortening in the latest Jurassic and earliest Cretaceous. Horizontal shortening would mark an initial period of contraction and folding during the early post-rift phase, leading to the syn-tectonic growth of sedimentary wedges at anticline and outcrop scales (Figs. 4 & 5). Shortening would have started during latest Jurassic – earliest Cretaceous (J-C) and continued during the deposition of the Lower Cretaceous unit (C1), and finally ended before unit C3 deposition. During this time, the Jbel Amsittene developed as an open anticline that was probably asymmetrical along strike. The Triassic salt would function as a weak detachment facilitating accommodation of the horizontal stresses that lead to the reactivation of pre-existing structures (e.g., basement rift-related faults) and initial anticline growth before Cretaceous-Cenozoic tectonics (Hafid et al. 2006; Tari et al. 2003; Hafid 2006). This shortening tectonics would be consistent with field observations of syn-sedimentary structures in the J-C unit as well as the existence of structures with clear vergence tens of meters away from the outcropping salt with limited strain (Fig. 3) near its contact. The lack of coherency in trend or scale of the salt with the overall anticline structure are also indicators of absence of halokinesis in the Jbel Amsittene during early post-rift of the Central Atlantic. These observations imply that Triassic salts were mobilised during compression led by horizontal tectonic forces, and that the growth of associated structures occurred in relation to a blind thrust rooted in the Triassic salt. The tête-plongeante structure towards the west and overturned layers at some sites indicate further shortening and anticline tightening during Alpine times. These structures and their consistent change along strike (Fig. 7) argue for vertical anticline growth during two overprinting phases of shortening, both acting roughly in the N-S direction. We thus consider that the evidence reported here favors the second scenario by which the latest Jurassic – earliest Cretaceous growth of the Jbel Amsittene occurred by tectonic shortening.

The ENE-WSW strike of the Jbel Amsittene Anticline is parallel to the strike of the major structures bounding the High Atlas belt (Fig. 1B). These structures activated under a transtensional regime during the Triassic-Early Jurassic rifting, and defined several pull-apart basins where grabens and half-grabens, bounded by N- to NE-trending normal faults related to rifting of the Central Atlantic, were filled by terrigenous and evaporitic series (Piqué et al. 2002; Laville et al. 2004; Frizon de Lamotte 2005). In our attempt to reconstruct the evolution of the Jbel Amsittene through time, we hypothesize that the Jbel Amsittene Anticline formed in strata overlying a previous graben structure bounded by an E-dipping normal fault to the east and a E-W transform fault to the north (Figs. 1B & 9). The latter is shown in the Mesozoic structural map of the Essaouira-Agadir Basin by LeRoy & Pique (2001), based on seismic data. The presence and relative accommodation space expected from both these pre-existing structures could explain increasing Jurassic thicknesses westwards and northwards along and across anticline strike, respectively (Figs. 7 & 8). We interpret the upwards decreasing thickness in Upper Jurassic units (Fig. 9) as an indication that the aforementioned faults were sealed, at the latest, by the end of the Late Jurassic (rifting kinematics, for both High Atlas and Central Atlantic, end in the Early Jurassic; e.g., Michard et al. 2008). Subsequent Late Jurassic-Early Cretaceous folding of the Jbel Amsittene Anticline may have occurred by reactivation of the E-W structure as a blind thrust, as interpreted on the structural map of Hafid et al., (2006) and on their seismic interpretation. This would result in thicknesses that increase towards the hanging-wall, i.e. southwards across the anticline, and are thus opposite in trend with regards to those in the Jurassic units (Table 2). Such blind thrust would be rooted in Triassic evaporites, acting as a weak decollement layer between the basement and the overlying Mesozoic basin infill (Fig. 9). Therefore, most of the strain was localised in the depocentre of the Triassic salt found underneath the western part of the Jbel Amsittene and wedging out towards the east. This is coherent with eastwards decreasing strain observed for both the early post-rift and the Alpine shortening phases.

Figure 9. Evolutionary model of the Jbel Amsittene Anticline. *Proposed evolutionary model of the Jbel Amsittene Anticline. In the last time-step we show the anticline with its finite geometry at present, which also results from Alpine tectonism.*

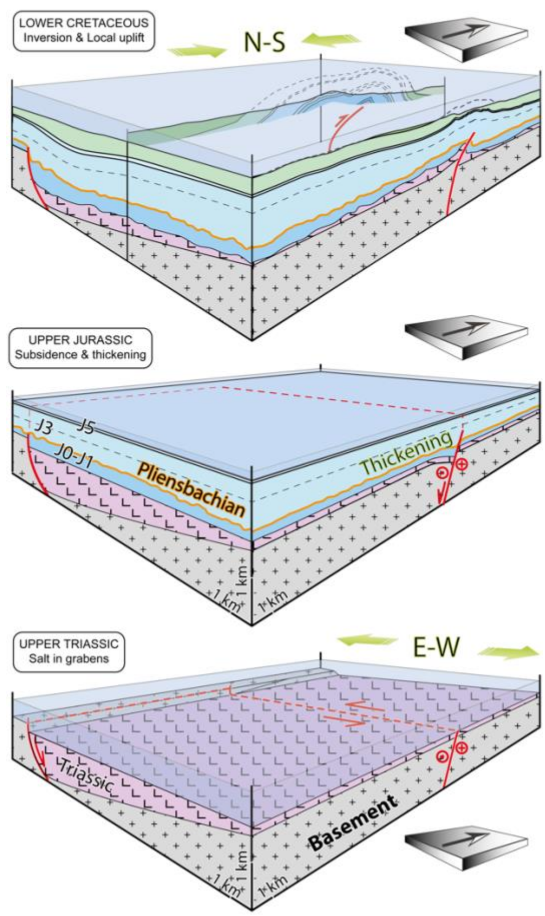

4.3 Regional shortening in other Moroccan sites during anticline growth

Observations within and nearby the Essaouira-Agadir Basin, suggest that some of the other salt structures present in the rifted margin may have been originally formed at earlier times than the Tertiary contraction (Hafid et al. 2006; e.g., Bertotti and Gouiza 2012; Saura et al. 2013; Benvenuti et al. 2017; Moragas et al. 2018; Pichel et al. 2019a). This could be the case of the Tidsi Anticline and the Imi n'Tanout wedge in the Essaouira-Agadir Basin (Fig. 1B), and the Dadès Valley in the Ouarzazate Basin. These structures may have formed similarly to the Jbel Amsittene Anticline, i.e. during an early post-rift shortening phase that reactivated inherited structures in assistance of the Triassic evaporitic rocks (Fig. 9). However, truncation of the basalt horizons by the Pliensbachian unconformity within certain structures also suggest the presence of earlier salt growth (Hafid et al. 2006).

The Tidsi Anticline, north of the Jbel Amsittene Anticline (Fig. 1B), was also thought to result from salt diapirism during the Late Cretaceous. The main arguments are the presence of growth strata documented in the Upper Cretaceous rocks and the lack of Jurassic series, coupled with the absence of tectonic indicators associated with these growth features (Amrhar 1995; Hafid 2006). While the relevance of diapirism in controlling the growth of the Tidsi Anticline during Late Cretaceous time is not unlikely, other older structures are observed in the area which document the existence of Early Cretaceous tectonic deformations hitherto neglected (Bertotti and Gouiza 2012). The best structures are visible along a >1 km long cliff in the southern part of the Tidsi Anticline where Triassic to Cretaceous sediments outcrop. A wedge is readily delineated by Lower Cretaceous rocks. The wedge opens southwards and is bounded on the southern side by steeper layers showing folded Early Lower Cretaceous beds along a WNW-ESE to NW-SE axis parallel to the strike of the wedge. Strata geometry suggest that this structure has NNE-ward vergence. Late Lower Cretaceous strata in the uppermost part of the outcrop are sub-horizontal, documenting the pre-Late Cretaceous age of deformation (Bertotti and Gouiza 2012). The tectonic nature of these structures is not only suggested by their overall geometry but is also proven by the fold vergence towards the core of the Tidsi Anticline, which is incompatible with an halokinetic origin.

To the east of Jbel Amsittene, the geometry of the post-rift portion of the Imi n'Tanout wedge (Fig. 1B) prior to Alpine shortening was previously reconstructed coupling thickness measurements with structural field observations (Zühlke et al. 2004; Bertotti and Gouiza 2012). The post-rift strata show a gradual increase in thickness from NE to SW, reaching more than 3000 m towards the coastal areas and indicating that the Imi n'Tanout wedge opened along a NNW-SSE to NW-SE trending axis. Fieldwork observations in the Imi n'Tanout region reveal the presence of two sets of shortening structures (Bertotti and Gouiza 2012). An older set oriented NW-SE to WNW-ESE is documented by syn-sedimentary thrust and fold structures that affect Middle Jurassic to Lower Cretaceous sediments to the south of the Imi n'Tanout line (see arguments in Bertotti and Gouiza 2012). At the outcrop-scale, syn-depositional deformation is common in the Imi n'Tanout wedge and typically show folds and thrusts with a NW-SE trending axis. All these structures document Late Jurassic to Early Cretaceous NE-SW shortening approximately perpendicular to the axis of the Imi n'Tanout wedge suggesting their formation within the same deformation regime. The younger set, oriented E-W to WSW-ENE, is found mainly in the Cretaceous sediments to the N of the Imi n'Tanout line and characterized by symmetrical to vergent folds. This set is conformal to the large-scale folds in the northern part of the Essaouira-Agadir Basin that are related to the inversion of the Atlas system.

In the Ouarzazate foreland basin, located ca. 300 km southeast of the Essaouira-Agadir Basin and south of the central High Atlas (Fig. 1A), there is also strong evidence for a pre-Atlasic shortening event (Benvenuti et al. 2017). Observations from the Dadès Valley indicate angular and progressive unconformities of syn-tectonic character within the Middle Jurassic to Lower Cretaceous stratigraphic units (Benvenuti et al. 2017). In addition, syn-sedimentary tectonic structures are also documented , thus suggesting a first Middle Jurassic-Early Cretaceous NNE-SSW to NNW-SSE shortening and a later E-W shortening during the Late Cretaceous (Benvenuti et al. 2017).

4.4 Vertical motions and horizontal deformations during anticline growth

A review of the temporal and spatial distribution of the crustal vertical movements has led to the proposal of an overall exhumation/subsidence history for Morocco and its surroundings (Charton et al. 2018). Present-day basement massifs surrounding the Essaouira-Agadir Basin, i.e. the Anti-Atlas, the Marrakech High Atlas, and the Meseta, have been active sources of sediments sporadically throughout the Mesozoic (Fig. 10). Specifically, the Anti-Atlas, south of the Jbel Amsittene area underwent significant exhumation between the Triassic and Middle Jurassic and during the Late Cretaceous to Present-day, while the Meseta and High Atlas massifs were exhumed from the Middle Jurassic to the Early Cretaceous and towards the end of the Late Cretaceous. This discrepancy in exhumation time led to substantial shifts in source areas, yet to be tested with sedimentary provenance analysis in the Essaouira-Agadir Basin.

Contractional structures in the Cretaceous sedimentary units of the Essaouira-Agadir Basin are coeval with major rearrangements in plate motions related to the opening of the South and North Atlantic Ocean (Fig 10). Continental separation and accretion of oceanic crust in the South Atlantic (Torsvik et al. 2009), between SW Africa and South America, as well as in the southern segment of the North Atlantic (Knott et al. 1993; Tucholke et al. 2007), between Iberia and Newfoundland, started in the Aptian-Albian time. We propose that the resulting counterclockwise rotation of Africa and the southward drifting of Iberia led to N-S compressive stresses within the African plate. At the same time, the ongoing oceanic accretion and mid-Atlantic ridge push in the Central Atlantic resulted in E-W compressive stresses (e.g., Gouiza et al. 2019). Complementarily, another Mesozoic failed rift system between northwest and southern Africa along the Atlantic margin was active in the Early Cretaceous (e.g., Guiraud and Maurin 1992) that may have triggered N-S far-field stresses in Morocco.

The steady acceleration of the Atlantic Mid-Oceanic ridge spreading during the Jurassic period is a known active process in the Central-Atlantic region that may lead to tectonic stresses (Fig. 10C; Labails et al., 2010). Several drivers of the erosional exhumation were at work in the Jurassic: (a) relatively low sea level (e.g., Snedden and Liu, 2010); (b) far-field intraplate stresses by Mid Oceanic Ridge push; (c) positive dynamic topography (up to 100 m of surface uplift; Barnett-Moore et al. 2017) potentially leading to regional instabilities; (d) high paleo-latitudes (similar to those of the Present-day; after Scotese 2016; Fig. 10C) and; (e) arid to humid climates in the High Atlas during the Early Jurassic (Wilmsen and Neuweiler 2007). Some of these processes, or some combination of them, may be responsible for the documented exhumation, and could have resulted in the instability and mobilisation of the Triassic salt by erosion of the sedimentary cap, generating hydraulic heads from East to West with surface uplifts in the surrounding massifs, or the propagation of faults in the salt cap generated by far-field intraplate stresses and/or surface uplift.

Figure 10. Time chart and compilation for the Jbel Amsittene Anticline. *(A) Tectonic events (after Charton 2018 and the references therein); (B) Sea level (after Snedden and Liu 2010); (C) Paleolatitude (after maps of Scotese 2016); (D) Full mid oceanic ridge spreading rates (compiled in Charton 2018); (E) Dynamic topography for two points in Morocco (from GPlates website, after modle CIs of Barnett-Moore et al. (2017); (F) Exhumation events as compiled in Charton (2018; see references therein); (G) Evolution of the Jbel Amsittene (this work).*

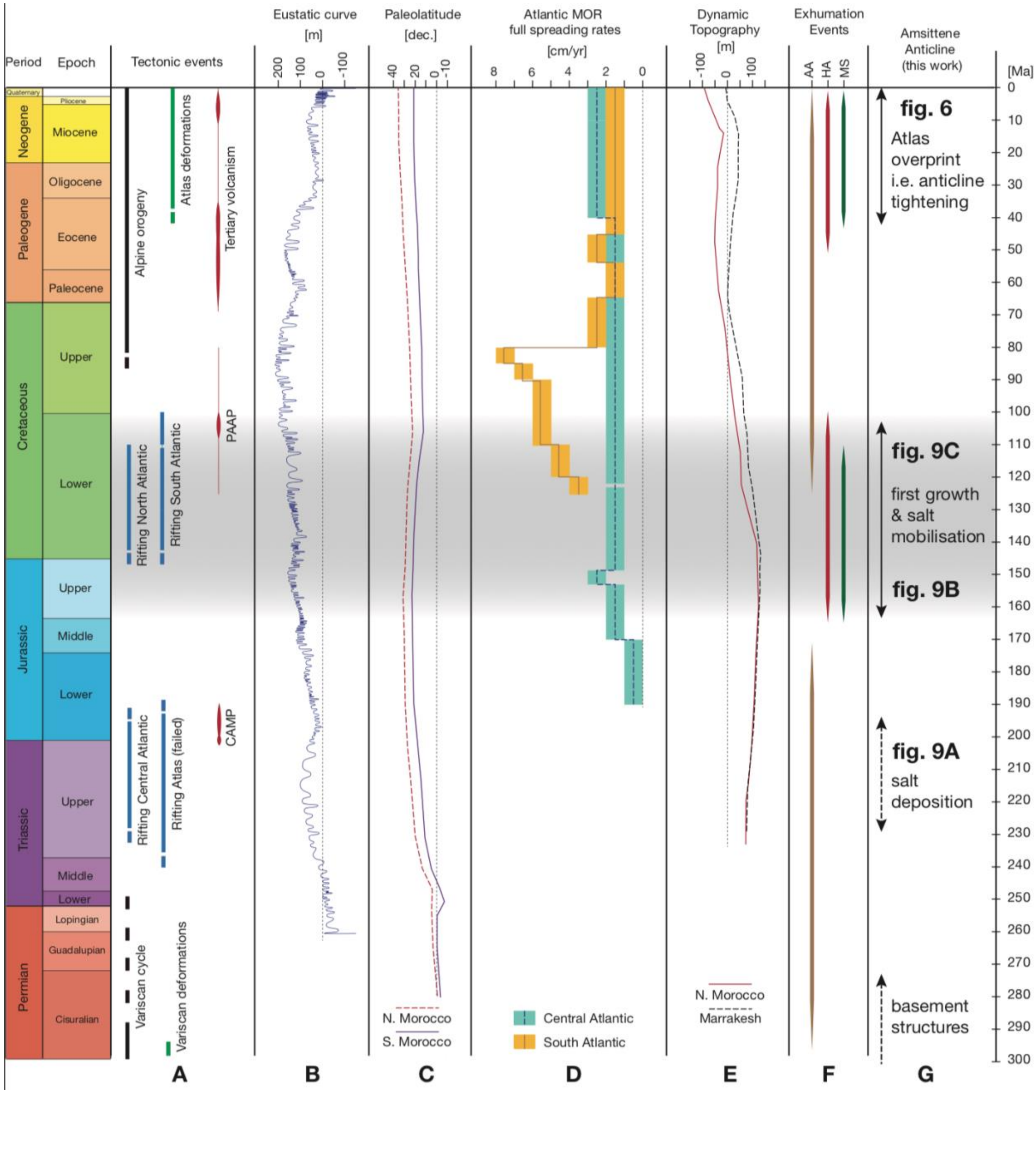

The spatial and temporal relation between these contractional structures and the regional uplift event that affected the NW African margin suggest a common genetic process (Ghorbal et al. 2008; Leprêtre et al. 2015b; Gouiza et al. 2017b; Charton et al. 2018). We consider that Late Jurassic-Early Cretaceous shortening in the Essaouira-Agadir Basin was driven by these N-S and E-W compressive stresses that reactivated the E-W (High Atlas/Tethysian failed rift) and N-S (Central Atlantic rift) syn-rift structures alike, and later initiated subsequent salt movements onshore and offshore the Moroccan rifted margin (Hafid et al. 2006; Hafid 2000, 2006; Tari et al. 2003).

5. Conclusions

We collected detailed structural evidence in the Jbel Amsittene. Our data indicates that the structure is an asymmetrical and north-verging anticline, with a northern flank that dips steeply and locally overturns, and a southern flank that dips south more gently. Our data suggest that the Jbel Amsittene Anticline is a fault-propagation-fold with its detachment plane rooted in Late Triassic evaporites, that initially grew during NNW-SSE shortening by the end of the Late Jurassic. Shortening led to anticline-scale and outcrop-scale syn-tectonic wedges in Late Jurassic and Early Cretaceous strata and outcrop-scale syn-sedimentary structures indicating compressional stresses. The anticline lacks structures related to diapiric rise at relevant scales and the effect of salt diapirism is restricted locally to an area around the anticline core. We therefore conclude that the initial development of Jbel Amsittene Ancline during Late Jurassic-Early Cretaceous times was mainly driven by shortening led by compressional tectonics, and only partially the result of salt tectonics, despite the promotion of halokinetic drivers described in recent literature. Later inversion of the Atlas system since the Late Cretaceous caused the tightening of the anticline. Being one of many contemporaneous contractional structures reported in the Essaouira-Agadir Basin and nearby basins linked to crustal-scale Middle Jurassic to Early Cretaceous exhumation, our observations suggest a tectonic evolution driven by intraplate stresses along the entire NW African margin.

Acknowledgements

Authors would like to thank the careful reviews by two anonymous colleagues on a previous version of the manuscript. DFB wants to thank the Vrije Universiteit Amsterdam for funds that partially covered fieldwork expenses of this work, part of his M.Sc. Thesis.

Figures

Figure 1. Maps of tectonic provinces and geology. (A) Regional map of Morocco showing the major tectono-stratigraphic provinces and basins of coastal Western Morocco (simplified from the geological map of Morocco; Hollard et al. 1985). With indication of the location of Panel B. **(B)** Geological map of the western High Atlas and Essaouira-Agadir Basin showing the main Triassic-Liassic rift-related structures near the Amsittene Anticline (Hollard et al. 1985; Le Roy and Piqué 2001).

Figure 2. Geology and chronostratigraphy in the Jbel Amsittene Anticline. (A) Geological map of the Jbel Amsittene Anticline, showing the location of the main observations in the field and cross-sections that have been used to constrain the geological evolution of the area. Outcrops and outcrop numbers are shown as Oc.#. **(B)** Simplified chronostratigraphic and environmental column of the Jbel Amsittene area. Based on Hafid (2000), the geological map of Tamanar from the Moroccan Geological Survey and Zühlke et al. (2004).

Figure 3. Western profile and main outcrops. (A) Cross-section A. **(B)** Outcrop 1. Limestones with regional bedding shown in yellow and faults and fault planes shown in red, with striae in dashed stroke. Conjugate sets and their stress directions indicate a north to south to north-northeast to south-southwest

shortening. The steepness of the faults may indicate reactivation. **(C)** Outcrop 2. Neptunian clastic dyke of calcarenite shown in red intruded in limestone with regional bedding shown in yellow. The neptunian dyke has a present position of 272/83. Assuming horizontal bedding at the moment of deposition, the neptunian dyke developed vertically, and is an indicator of east-west extension. **(D)** Outcrop 3. Folded and faulted soft sediments in a syn-sedimentary ramp fold, verging north, indicating shortening in a 160-340 direction during the 144-150 Ma (latest Jurassic). Limestone showing regional bedding to the left and folded strata to the right (in yellow) and a reverse fault (in red). The soft sedimentary packet (with a sedimentary pattern) shows a chaotic character with no evidence of brechiation. **(E)** Outcrop 4. Map of the salt outcrop in the west and adjacent formations, showing the bedding strikes around the evaporitic body. **(F)** Outcrop 5. Reverse faults and folds with southeastern vergence, in a limestone outcrop situated less than 200 meters east of the outcropping salt. Regional bedding to the right and folded strata to the left are shown in yellow and reverse faults are shown in red. Rocks in the outcrop are not affected by halokinesis, and show signs of compressional deformation. The orientation of the fault planes and the axial planes of the folds are similar and indicate NNW-SSE shortening.

Figure 4. Central profile and main outcrops. (A) Cross-section B. **(B)** Outcrop 6. Meter-scale fold in limestones at the location of main dip change in beds (shown in yellow) at the anticline axis. **(C)** Outcrop 7. Underthrust in overturned limestone strata. The fault is in red and beds are in yellow. Fault-bend fold, with top to the south movement, with 175/73 regional bedding. The fold in the hanging wall has a fold axis of 085/06 and axial plane of 022/14.

Figure 5. Eastern profile and main outcrops. (A) Cross-section C. **(B)** Outcrop 8. Inclined limestone layers cut by synsedimentary faults. High-angle reverse faults (in red) transect a thick bank (with its top and its bottom beds in yellow) with an offset of ~20 cm. The reverse fault tips end in the sedimentary layer on top that show soft sediment deformation of chaotic nature (in thin black), bracketing the age of

deformation to 146-137 Ma (J-C formation, lowermost Lower Cretaceous – uppermost Lower Jurassic). The inclination of the reverse faults is suggestive of reactivation of former normal faults. **(C)** Outcrop 9. One of the two sets of sigmoidal tension gashes that outcrop at both sides of one of the anticline axes, in limestones. They indicate right lateral shear.

Figure 6. Outcrop 10. Limestone outcrop showing an approximately 30 m long wedge pinching out towards the south, overlaying faulted strata. The top to the north-northeast faults have reverse offsets of a few to tens of centimetres that do not continue into the wedge, indicating a shortening direction of SSW-NNE during the J-C formation, lowermost Lower Cretaceous – uppermost Lower Jurassic. The steepness of the faults may be indicative of reactivation.

Figure 7. Structure of the Jbel Amsittene Anticline. (A) Structural map showing the main axis of the anticline, which bifurcate westwards, and its plunge towards the east. The also shows regional bed attitude representative of different sectors of the anticline. We provide all bed dip data from the fieldwork in the Supplementary Materials. Contours in grey represent lines of equal height every 50 m, with darker tones and thicker strokes for the heights of 250 m, 500 m and 750 m. **(B)** Geological profiles in the Jbel Amsittene Anticline, from west to east, showing the anticline structure and vergence and its lateral variations.

Figure 8. Thickness model. (A/B/C) Model of thickness variations along contour likes of three Upper Jurassic sequences. **(D)** Modelled thickness variations of Jurassic rocks in a clockwise profile from the northwestern to the southwestern flank of the anticline.

Figure 9. Evolutionary model of the Jbel Amsittene Anticline. Proposed evolutionary model of the Jbel Amsittene Anticline. In the last time-step we show the anticline with its finite geometry at present, which also results from Alpine tectonism.

Figure 10. Time chart and compilation for the Jbel Amsittene Anticline. (A) Tectonic events (after Charton 2018 and the references therein); **(B)** Sea level (after Snedden and Liu 2010)**; (C)** Paleolatitude (after maps of Scotese 2016); **(D)** Full mid oceanic ridge spreading rates (compiled in Charton 2018); **(E)** Dynamic topography for two points in Morocco (from GPlates website, after modle CIs of Barnett-Moore et al. (2017); **(F)** Exhumation events as compiled in Charton (2018; see references therein); **(G)** Evolution of the Jbel Amsittene (this work).

Tables

Table 1. Orientation of the main stresses derived from Outcrop 1 (Fig. 3B).

Table 2. Thickness changes between the northern and the southern flank of the Jbel Amsittene Anticline for formations J-C and C1.

Table 3. Decrease in amount of shortening to the east, measured as unfolded line-length.

References

Amrhar M (1995) Évolution structurale du Haut Atlas occidental dans le cadre de l'ouverture de l'Atlantique centrale et de la collision Afrique--Europe: Structure, instabilités tectoniques et magmatisme. Thèse Doct. Etat, Univ. Cadi Ayyad, Marrakech

Barnett-Moore N, Hassan R, Müller RD, et al (2017) Dynamic topography and eustasy controlled the paleogeographic evolution of northern Africa since the mid-Cretaceous: DYNAMIC TOPOGRAPHY IN NORTHERN AFRICA. Tectonics 36:929–944

Bennison G, Moseley K (2003) An Introduction to Geological Structures and Maps 7ed

Benvenuti M, Moratti G, Algouti A (2017) Stratigraphic and structural revision of the Upper Mesozoic succession of the Dadès valley, eastern Ouarzazate Basin (Morocco). J Afr Earth Sci 135:54–71

Bertotti G, Gouiza M (2012) Post-rift vertical movements and horizontal deformations in the eastern margin of the Central Atlantic: Middle Jurassic to Early Cretaceous evolution of Morocco. Int J Earth Sci 101:2151–2165

Bonow JM, Japsen P, Green PF, et al (2009) Post-rift landscape development of north-east Brazil. Geological Survey of Denmark and Greenland Bulletin 17:81–84

Charton R, Bertotti G, Arantegui A, Bulot L (2018) The Sidi Ifni transect across the rifted margin of Morocco (Central Atlantic): Vertical movements constrained by low-temperature thermochronology. J Afr Earth Sci 141:22–32

Charton RJG (2018) Phanerozoic Vertical Movements in Morocco. Delft University of Technology

Duffaud F, Brun L, Plauchut B (1966) Le bassin du Sud-Ouest marocain. Bassins sédimentaires du littoral Africain Publ Assoc Serv Géol Afric 1:5–26

Duval-Arnould A (2019) Controls on stratigraphic development of shelf margin carbonates: Jurassic Atlantic margin - Essaouira-Agadir Basin, Western Morocco. Doctoral Thesis, Manchester University

Ellouz N, Patriat M, Gaulier J-M, et al (2003) From rifting to Alpine inversion: Mesozoic and Cenozoic subsidence history of some Moroccan basins. Sediment Geol 156:185–212

Frizon de Lamotte D (2005) About the Cenozoic inversion of the Atlas domain in North Africa. C R Geosci 337:475–476

Frizon de Lamotte D, Andrieux J, Guezou JC (1991) Cinematique des chevauchements neogenes dans l'Arc betico-rifain; discussion sur les modeles geodynamiques. Bull Soc Geol Fr 162:611–626

Frizon de Lamotte D, Saint Bezar B, Bracène R, Mercier E (2000) The two main steps of the Atlas building and geodynamics of the western Mediterranean. Tectonics 19:740–761

Frizon de Lamotte D, Zizi M, Missenard Y, et al (2008) The Atlas System. In: Michard A, Saddiqi O, Chalouan A, de Lamotte DF (eds) Continental Evolution: The Geology of Morocco. Springer Nature, Berlin Heidelberg, pp 133–202

Ghorbal B (2009) Mesozoic to Quaternary thermo-tectonic evolution of Morocco (NW Africa). Vrije

Universiteit Amsterdam

Ghorbal B, Bertotti G, Foeken J, Andriessen P (2008) Unexpected Jurassic to Neogene vertical movements in “stable” parts of NW Africa revealed by low temperature geochronology. Terra Nova 20:355–363

Giles KA, Lawton TF (2002) Halokinetic Sequence Stratigraphy Adjacent to the El Papalote Diapir, Northeastern Mexico. AAPG Bull 86:823–840

Gouiza M (2011) Mesozoic Source-to-Sink Systems in NW Africa:: Geology of vertical movements during the birth and growth of the Moroccan rifted margin. Vrije Universiteit Amsterdam

Gouiza M, Bertotti G, Andriessen PAM (2017a) Mesozoic and Cenozoic thermal history of the western Reguibat Shield (West African Craton). Terra Nova. https://doi.org/10.1111/ter.12318

Gouiza M, Bertotti G, Charton R, et al (2019) New Evidence of “Anomalous” Vertical Movements along the Hinterland of the Atlantic NW African Margin. J Geophys Res [Solid Earth]. https://doi.org/10.1029/2019JB017914

Gouiza M, Charton R, Bertotti G, et al (2017b) Post-Variscan evolution of the Anti-Atlas belt of Morocco constrained from low-temperature geochronology. Int J Earth Sci 106:593–616

Green PF, Japsen P, Chalmers JA, et al (2018) Post-breakup burial and exhumation of passive continental margins: Seven propositions to inform geodynamic models. Gondwana Res 53:58–81

Guiraud R, Maurin J-C (1992) Early Cretaceous rifts of Western and Central Africa: an overview. Tectonophysics 213:153–168

Hafid M (2000) Triassic–early Liassic extensional systems and their Tertiary inversion, Essaouira Basin (Morocco). Mar Pet Geol 17:409–429

Hafid M (2006) Styles structuraux du Haut Atlas de Cap Tafelney et de la partie septentrionale du Haut Atlas occidental: tectonique salifère et relation entre l’Atlas et l’Atlantique. Notes Mém Serv Géol Maroc 465:172

Hafid M, Zizi M, Bally AW, Ait Salem A (2006) Structural styles of the western onshore and offshore termination of the High Atlas, Morocco. C R Geosci 338:50–64

Hoggard MJ, White N, Al-Attar D (2016) Global dynamic topography observations reveal limited influence of large-scale mantle flow. Nat Geosci 9:456

Hollard H, Choubert G, Bronner G, et al (1985) Carte géologique du Maroc, Geological map: Rabat, Morocco. Service Géologique du Maroc

Jaïdi S, Bencheqroun A, Diouri M (1970) Carte Géologique du Maroc 1:100 000, Feuille Tamanar. Not Mém Serv Géol Maroc 201:

Japsen P, Bonow JM, Green PF, et al (2006) Elevated, passive continental margins: Long-term highs or Neogene uplifts? New evidence from West Greenland. Earth Planet Sci Lett 248:330–339

Japsen P, Bonow JM, Green PF, et al (2009) Formation, uplift and dissection of planation surfaces at passive continental margins – a new approach. Earth Surf Processes Landforms 34:683–699

Japsen P, Chalmers JA (2000) Neogene uplift and tectonics around the North Atlantic: overview. Glob Planet Change 24:165–173

Japsen P, Chalmers JA, Green PF, Bonow JM (2012) Elevated, passive continental margins: Not rift shoulders, but expressions of episodic, post-rift burial and exhumation. Glob Planet Change 90-91:73–86

Klitgord KD, Schouten H (1986) Plate kinematics of the central Atlantic. The Geology of North America 1000:351–378

Knott SD, Burchell MT, Jolley EJ, Fraser AJ (1993) Mesozoic to Cenozoic plate reconstructions of the North Atlantic and hydrocarbon plays of the Atlantic margins. In: Petroleum Geology of Northwest Europe: Proceedings of the 4th Conference. Geological Society of London, pp 953–974

Laville E, Piqué A (1992) Jurassic penetrative deformation and Cenozoic uplift in the Central High Atlas (Morocco): A tectonic model. structural and orogenic inversions. Geol Rundsch 81:157–170

Laville E, Pique A, Amrhar M, Charroud M (2004) A restatement of the Mesozoic Atlasic Rifting (Morocco). J Afr Earth Sci 38:145–153

Leprêtre R, Missenard Y, Barbarand J, et al (2015a) Postrift history of the eastern central Atlantic passive margin: Insights from the Saharan region of South Morocco. J Geophys Res [Solid Earth] 120:2014JB011549

Leprêtre R, Missenard Y, Saint-Bezar B, et al (2015b) The three main steps of the Marrakech High Atlas building in Morocco: Structural evidences from the southern foreland, Imini area. J Afr Earth Sci 109:177–194

Le Roy P, Piqué A (2001) Triassic–Liassic Western Moroccan synrift basins in relation to the Central Atlantic opening. Mar Geol 172:359–381

Luber TL, Bulot LG, Redfern J, et al (2019) A revised chronostratigraphic framework for the Aptian of the Essaouira-Agadir Basin, a candidate type section for the NW African Atlantic Margin. Cretaceous Res 93:292–317

Malusà MG, Polino R, Feroni AC, et al (2007) Post-Variscan tectonics in eastern Anti-Atlas (Morocco). Terra Nova 19:481–489

Medina F (1995) Syn- and postrift evolution of the El Jadida – Agadir basin (Morocco): constraints for the rifting models of the central Atlantic. Can J Earth Sci 32:1273–1291

Michard A, Saddiqi O, Chalouan A, de Lamotte DF (2008) Continental Evolution: The Geology of Morocco: Structure, Stratigraphy, and Tectonics of the Africa-Atlantic-Mediterranean Triple Junction. Springer

Moragas M, Vergés J, Saura E, et al (2018) Jurassic rifting to post-rift subsidence analysis in the Central High Atlas and its relation to salt diapirism. Basin Res 30:336–362

Morley CK, Crevello P, Ahmad ZH (1998) Shale tectonics and deformation associated with active diapirism: the Jerudong Anticline, Brunei Darussalam. J Geol Soc London 155:475–490

Müller RD, Hassan R, Gurnis M, et al (2018) Dynamic topography of passive continental margins and their hinterlands since the Cretaceous. Gondwana Research 53:225–251

Neumaier M, Back S, Littke R, et al (2016) Late Cretaceous to Cenozoic geodynamic evolution of the Atlantic margin offshore Essaouira (Morocco). Basin Res 28:712–730

Ouajhain B, Daoudi L, Laduron D, et al (2011) Jurassic clay mineral sedimentation control factors in the Essaouira Basin (Western High Atlas, Morocco). Geologica Belgica

Oukassou M, Saddiqi O, Barbarand J, et al (2013) Post-Variscan exhumation of the Central Anti-Atlas (Morocco) constrained by zircon and apatite fission-track thermochronology. Terra Nova 25:151–159

Peulvast J-P, Claudino Sales V, Bétard F, Gunnell Y (2008) Low post-Cenomanian denudation depths across the Brazilian Northeast: Implications for long-term landscape evolution at a transform continental margin. Glob Planet Change 62:39–60

Pichel LM, Finch E, Gawthorpe RL (2019a) The Impact of Pre-Salt Rift Topography on Salt Tectonics: A Discrete-Element Modeling Approach. Tectonics

Pichel LM, Huuse M, Redfern J, Finch E (2019b) The influence of base-salt relief, rift topography and regional events on salt tectonics offshore Morocco. Mar Pet Geol 103:87–113

Piqué A, Le Roy P, Amrhar M (1998) Transtensive synsedimentary tectonics associated with ocean opening: the Essaouira–Agadir segment of the Moroccan Atlantic margin. J Geol Soc London 155:913–928

Piqué A, Tricart P, Guiraud R, et al (2002) The Mesozoic-Cenozoic Atlas belt (North Africa): an overview. Geodin Acta 15:185–208

Poprawski Y, Basile C, Agirrezabala LM, et al (2014) Sedimentary and structural record of the Albian growth of the Bakio salt diapir (the Basque Country, northern Spain). Basin Res 26:746–766

Ruiz G, Sebti S, Negro F, et al (2011) From central Atlantic continental rift to Neogene uplift--western Anti-Atlas (Morocco). Terra Nova 23:35–41

Saddiqi O, El Haimer F-Z, Michard A, et al (2009) Apatite fission-track analyses on basement granites from south-western Meseta, Morocco: Paleogeographic implications and interpretation of AFT age discrepancies. Tectonophysics 475:29–37

Sahabi M, Aslanian D, Olivet J-L (2004) Un nouveau point de départ pour l’histoire de l'Atlantique central. C R Geosci 336:1041–1052

Saura E, Vergés J, Martín-Martín JD, et al (2013) Syn- to post-rift diapirism and minibasins of the Central High Atlas (Morocco): the changing face of a mountain belt. J Geol Soc London 171:97–105

Scotese C (2016) PALEOMAP: Paleoatlas for GPlates and the paleodataplotter program

Seguret M (1972) Étude tectonique des nappes et séries décollées de la partie centrale des Pyrénées. Thesis. Science Univ. Montpellier

Sehrt M (2014) Variscan to Neogene long-term landscape evolution at the Moroccan passive continental margin (Tarfaya Basin and western Anti-Atlas). Heidelberg

Snedden JW, Liu C (2010) A compilation of Phanerozoic sea-level change, coastal onlaps and recommended sequence designations. Search and discovery article 40594:3

Stets J (1992) Mid-Jurassic events in the Western High Atlas (Morocco). Geol Rundsch 81:69–84

Tari G, Molnar J, Ashton P (2003) Examples of salt tectonics from West Africa: a comparative approach. Geological Society, London, Special Publications 207:85–104

Teixell A, Arboleya M-L, Julivert M, Charroud M (2003) Tectonic shortening and topography in the central High Atlas (Morocco). Tectonics 22:1051

Torsvik TH, Rousse S, Labails C, Smethurst MA (2009) A new scheme for the opening of the South Atlantic Ocean and the dissection of an Aptian salt basin. Geophys J Int 177:1315–1333

Tucholke BE, Sawyer DS, Sibuet J-C (2007) Breakup of the Newfoundland–Iberia rift. Geological Society, London, Special Publications 282:9–46

Westaway R, Aït Hssaine A, Demir T, Beck A (2009) Field reconnaissance of the Anti-Atlas coastline, Morocco: Fluvial and marine evidence for Late Cenozoic uplift. Glob Planet Change 68:297–310

Wilmsen M, Neuweiler F (2007) Biosedimentology of the Early Jurassic post-extinction carbonate depositional system, central High Atlas rift basin, Morocco: Early Jurassic biosedimentology. Sedimentology 55:773–807

Zühlke R, Bouaouda M-S, Ouajhain B, et al (2004) Quantitative Meso-/Cenozoic development of the eastern Central Atlantic continental shelf, western High Atlas, Morocco. Mar Pet Geol 21:225–276